DEVELOPMENT OF AN ALL SPEED NAVIER-STOKES PRECONDITIONER FOR TWO AND THREE DIMENSIONAL FLOWS ON HYBRID GRIDS

A THESIS SUBMITTED TO
THE GRADUATE SCHOOL OF NATURAL AND APPLIED SCIENCES
OF
MIDDLE EAST TECHNICAL UNIVERSITY

BY

ONUR BAŞ

IN PARTIAL FULFILLMENT OF THE REQUIREMENTS
FOR
THE DEGREE OF DOCTOR OF PHILOSOPHY
IN
AEROSPACE ENGINEERING

JULY 2015

Approval of the thesis:

DEVELOPMENT OF AN ALL SPEED NAVIER-STOKES PRECONDITIONER FOR TWO AND THREE DIMENSIONAL FLOWS ON HYBRID GRIDS

submitted by **ONUR BAŞ** in partial fulfillment of the requirements for the degree of **Doctor of Philosophy in Aerospace Engineering Department, Middle East Technical University** by,

Prof. Dr. Gülbin Dural Ünver
Dean, Graduate School of **Natural and Applied Sciences** ______________

Prof. Dr. Ozan Tekinalp
Head of Department, **Aerospace Engineering** ______________

Prof. Dr. İsmail Hakkı Tuncer
Supervisor, **Aerospace Eng. Dept., METU** ______________

Examining Committee Members:

Prof. Dr. Yusuf ÖZYÖRÜK
Aerospace Engineering Department, METU ______________

Prof. Dr. İsmail Hakkı Tuncer
Aerospace Engineering Department, METU ______________

Prof. Dr. Ünver Kaynak
Mechanical Engineering Department, TOBB-ETU ______________

Assoc. Prof. Dr. Sinan EYİ
Aerospace Engineering Department, METU ______________

Assist. Prof. Dr. Cüneyt SERT
Mechanical Engineering Department, METU ______________

Date: ______________

I hereby declare that all information in this document has been obtained and presented in accordance with academic rules and ethical conduct. I also declare that, as required by these rules and conduct, I have fully cited and referenced all material and results that are not original to this work.

Name, Last Name: ONUR BAŞ

Signature :

ABSTRACT

DEVELOPMENT OF AN ALL SPEED NAVIER-STOKES PRECONDITIONER FOR TWO AND THREE DIMENSIONAL FLOWS ON HYBRID GRIDS

BAŞ, Onur
Ph.D., Department of Aerospace Engineering
Supervisor : Prof. Dr. İsmail Hakkı Tuncer

July 2015, 88 pages

In this study, a novel Mach uniform preconditioning method is developed for the solution of Euler/Navier-Stokes equations at subsonic and incompressible flow conditions. In contrast to the methods developed earlier in which the conservation of mass equation is preconditioned, the conservation of energy equation is preconditioned in the present method to enforce the divergence free constraint on the velocity field even at the limiting case of incompressible, zero Mach number flows. The proposed Mach-uniform preconditioning method does not have a singularity point at zero free-stream Mach number. The modified system of equations preserves the strong conservation form of the governing equations for compressible flows and recovers the artificial compressibility equations in the case of zero Mach number. Two and three dimensional preconditioned solvers are developed for validation and performance evaluation of the present formulation on a wide range of Mach number flows. The studied cases show the convergence acceleration, stability and accuracy of the present Mach uniform preconditioner in comparison to the non-preconditioned compressible flow solutions. The convergence acceleration achieved is similar to those of the well known preconditioned system of equations for low subsonic flows and to the artificial compressibility method for incompressible flows.

Keywords: Preconditioning, Artificial Compressibility Method, Mach Uniform Accuracy, All Speed, Three Dimensional

ÖZ

HİBRİT AĞLARDA İKİ VE ÜÇ BOYUTLU AKIŞLAR İÇİN TÜM HIZLARDA GEÇERLİ NAVİER-STOKES ÖNKOŞULLANDIRICI GELİŞTİRİLMESİ

BAŞ, Onur
Doktora, Havacılık ve Uzay Mühendisliği Bölümü
Tez Yöneticisi : Prof. Dr. İsmail Hakkı Tuncer

Temmuz 2015 , 88 sayfa

Bu çalışmada Mach sayısının değerinden bağımsız olarak, yüksek doğruluklu, ses-altı hızlarda ve sıkışamaz akış koşullarında Euler/Navier-Stokes denklemlerinin çözümü için yeni bir önkoşullandırma metodu geliştirilmiştir. Daha önce kütlenin korunumu denkleminin önkoşullandırıldığı metodların aksine, mevcut yöntemde enerjinin korunumu denklemi önkoşullandırılmıştır. Bu yöntem, sıfır serbest akım Mach sayısı dahil olmak üzere, sıkışamaz akış limitinde dahi hız alanında ıraksamayı önlemektedir. Önerilen Mach sayısından bağımsız metod sıfır Mach sayısında bir tekillik noktasına sahip değildir. Önkoşullandırılmış denklem seti sıkışabilir rejimlerde, sıkışabilir akış denklemlerinin güçlü korunum formuna sahip olup, sıfır Mach sayısı limitinde Yapay Sıkışabilirlik Metoduna dönüşmektedir. Geniş bir Mach sayısı aralığında önerilen formülasyonun doğrulanması ve performansının değerlendirilmesi amacı ile iki ve üç boyutlu önkoşul-

landırılmış çözücüler geliştirilmiştir. Gerçekleştirilen çalışmalar, önerilen Mach sayısından bağımsız önkoşullandırma metodunun, önkoşullandırılmamış sıkışabilir akış çözümlerine kıyasla yakınsama hızındaki artışı, kararlılığı ve doğruluğu göstermiştir. Elde edilen yakınsama hızı artışı düşük sesaltı hızlarda diğer iyi bilinen önkoşullandırılmış denklem sistemleri ile benzer olup, sıkışamaz akışlarda ise Yapay Sıkışabilirlik Metodu ile benzerdir.

Anahtar Kelimeler: Önkoşullandırma, Yapay Sıkışabilirlik Metodu, Mach Bağımsız Doğruluk, Tüm Hızlar, Üç Boyutlu

Dedicated to my family...

ACKNOWLEDGMENTS

I would like to express my gratitude to Prof. Dr. İsmail Hakkı TUNCER for his supervision and sharing his already developed in-house codes as the base solver for three dimensional part of this thesis.

I would like to thank Prof. Dr. Ünver KAYNAK and Prof. Dr. Yusuf ÖZYÖRÜK for their suggestions throughout the theoretical and numerical experimentation stages.

I would also like to thank to my colleagues and friends Dr. Ozan TUĞLUK, Kerem DENK, Samet Çaka ÇAKMAKÇIOĞLU and İsmail Ozan SERT for their friendship, support and inspiring technical discussions. I am also grateful to Dr. Ozan TUĞLUK for his continuous supervision on Linux systems and Dr. Nilay SEZER UZOL for her support.

I want to express my deepest thanks to my parents Fatma BAŞ, Ali BAŞ and brother Ulaş BAŞ for their spiritual support. I hope that I deserve their confidence.

I devote this thesis to my beloved wife Meryem Meltem TATLIER BAŞ who is the real joy and happiness of my life.

Finally, I owe a special thank to my daughter Doğa to whom this thesis is also devoted. She was far from being helpful on this thesis study whereas she always able to show what is really important and beautiful in life.

TABLE OF CONTENTS

LIST OF TABLES

TABLES

LIST OF FIGURES

FIGURES

LIST OF ABBREVIATIONS

ROMAN SYMBOLS

A	Boundary surface of control volume
c	Speed of sound
CFL	Courant Friedrichs Lewy number
E, F, G	Flux components
e_t	Total energy
J	Jacobian matrix
k	Thermal conductivity
M	Mach number
n	Normal direction
p	Pressure
Pr	Prandtl number
Q	Flow variables
r	Distance to an edge center
R	Right eigenvector
Re	Reynolds number
S	Entropy
t	Time
T	Temperature
u, v, w	Velocity components
V	Control volume
W	Characteristic variables

GREEK SYMBOLS

ρ	Density
γ	Heat capacity ratio
λ	Eigenvalue
Γ	Preconditioning matrix

δ	Artificial compressibility parameter
$\vec{R}$	Residual vector
Δ	Gradient
Φ	Limiting function
τ	Viscous stresses
Θ	Work of viscous stresses and heat conduction
μ	Dynamic viscosity
γ	Heat capacity ratio

SUBSCRIPTS

∞	Free stream
r	Reference
L	Left state
R	Right state
x, y, z	Directions
i	Edge number

CHAPTER 1

INTRODUCTION

1.1 Background

The conservation equations that govern the fluid flow are well known for centuries. As all physical laws, their validity are observed repeatedly on scientific experiments and observations for all flows where continuum assumption is applicable. On the other hand, analytical solutions of these equations are not possible for most of the engineering problems and numerical solutions are widely used. However, appropriate numerical methods have to be selected for different flow regimes such as incompressible, transonic/supersonic or hypersonic flows. As a result, many different flow solver algorithms and formulations have been developed. Nowadays there is an ongoing effort on unifying these methods.

The governing equations of fluid flow, namely the Navier-Stokes equations, represent an hyperbolic-parabolic character for all flow conditions which allows the classical time marching solution methods except very low speed cases. Low speed flow is a special regime when compared with others since in real life, the divergence free velocity field practically satisfied at all the times. This phenomenon comes from the fact that flow velocity becomes so small when compared to speed of sound or in other words, pressure waves travel infinitely fast when compared to flow speed. The variation of density both in time and space is negligible for low speed flows where the conservation of mass equation becomes elliptical. This character change from hyperbolic-parabolic to elliptical results in severe stability and accuracy problems on the widely used numerical methods developed for the solution of compressible flow equations.

When the incompressibility limit is approached, two major problems can be identified on numerical solution of the governing equations. They are known as the "cancellation" and the "eigenvalue disparity" problems. The former problem can be defined as; one or more of the terms in the governing equations gaining increased dominance over other terms which results in suppression of their effects. The latter problem reveals itself in the solution of the governing equations when the eigenvalues are analyzed. The increase in the ratio between the maximum and the minimum eigenvalues (condition number) as Mach number decreases is known as the "eigenvalue disparity". This problem makes the discrete system of governing equations stiff. The numerical solution algorithms become mostly ineffective and the obtained solutions become inaccurate.

1.2 Incompressible Flow Solution Methodologies

There are various formulations used for solution of incompressible flows [1], [2] which can be classified in three main categories, namely vorticity-stream function method, pressure based methods and density based methods.

In the vorticity-stream function method, the incompressible Navier-Stokes equations are reformulated in terms of vorticity and stream function which automatically satisfies the conservation of mass equation [3]. The local velocity components and pressure values are then obtained from the converged flow field. The boundary conditions are also reformulated in this method. Although this formulation is suitable for 2-D flows, its extension to 3-D flows is not possible since a unique stream function is not definite in 3-D flows. Different formulations such as vorticity-velocity formulation [4] are present in the literature but selection of boundary conditions become challenging in these methods [5].

The second major category is the Marker and Cell(MAC) Method due to Harlow and Welch [6], projection method due to Chorin [7] and Semi-Implicit Method for Pressure Linked Equations(SIMPLE) family formulations due to Patankar and Spalding [8] which are named as pressure based methods.

The MAC approach employs pressure Poisson equation [9] to satisfy the conservation of mass and it is the first method applying this formulation. The Poisson equation is obtained by taking the divergence of the conservation of momentum equation. However the MAC approach fails to restore the divergence free velocity field effectively and it is susceptible to errors introduced to the conservation of mass equation originating mostly from the boundary conditions.

The pressure projection method is developed by Chorin [7] and Temam [10] as another pressure based method. This method consists of two decoupled steps in which an intermediate velocity is firstly calculated from the conservation of momentum equations ignoring the gradient of the pressure field. Incompressibility constraint is not forced at this step. Later, gradient of the pressure is calculated from the pressure Poisson equation and employed which is named as the projection step.

By far, the most popular approaches in pressure based methods are the family of SIMPLE algorithms including the original algorithm which is proposed by Patankar and Spalding [8] and the modified versions such as SIMPLER [14], SIMPLEC [15], SIMPLEST [16] and PISO [17]. These methods make a first guess on the pressure field and get an approximation of the velocity field as the first step. After that, the obtained velocity field is used for correcting the pressure field to ensure the conservation of mass. The major differences between the variants come from the simplifications employed in these estimation and correction steps. Despite their empiricism, these methods are used extensively in the literature [11], [12], [13].

The third method includes the Artificial Compressibility Method(ACM) due to Chorin [18]. In the ACM, a pseudo-time derivative of pressure is added to the conservation of mass equation. The added term relaxes the infinite acoustic speed to a predefined finite value. The major advantage of the ACM over pressure based methods is its similarity to the conservative form of the compressible flow equations, as such it allows the use of advanced solution algorithms developed for the compressible flows. The ACM method is widely applied in the solution of incompressible flows [19], [20], [21], [22], [23]. This method is recognized to be the first preconditioning algorithm which will be elaborated in the next section.

All of these methods for incompressible flows have their own advantages and disadvantages which are described in [24] in details.

1.3 Solution Methodologies for All Speed Flows

In all speed solution methods, SIMPLE and Preconditioning Methods come forward. The SIMPLE algorithms were developed firstly and widely applied to various problems. Then preconditioning methods are introduced by Turkel [28].

1.3.1 SIMPLE Based Algorithms

The SIMPLE algorithm and its variants are firstly developed for incompressible flows. With increasing demand for unified solution methods for low and high subsonic flows, Karki and Patankar [25] modified the original SIMPLE algorithm to solve compressible flows. After this initial work, some variants of SIMPLE are also extended to high subsonic flows [26].

The major problem of SIMPLE and its derivatives on the compressible flow regime is the presence of primitive variables in the formulations. The flux vector based on these variables are discontinuous across shockwaves and therefore they are not differentiable. Although SIMPLE algorithms are effective on high speed subsonic flows, their performance deteriorate significantly in transonic and supersonic flows in comparison to the formulations based on the strong conservative forms of the governing equations. The study of McGuirk and Paige[27] is an example of the effort to improve the shock capturing capability of SIMPLE algorithm at transonic flows. The methodology used in this study is to employ conservative variables in the computation of mass fluxes instead of flow velocities as the new solution variables.

1.3.2 Preconditioning Methods

In 1987, the first systematic approach on preconditioning methods is conducted by Turkel [28] and a family of preconditioners are introduced. The preconditioning methods then gained increasing popularity in the development of all speed inviscid flow solvers. These methods employ special matrices which enhance the convergence behavior when pre-multiplied with the time derivative terms in the governing flow equations. The major goal of the preconditioning methods is to reduce the difference between the particle/flow speed and the acoustic wave speed. Although this technique modifies the magnitude of the eigenvalues, it retains the signs of the eigenvalues. The modified system of equations remain hyperbolic-parabolic for all Mach numbers.

The family of preconditioners introduced by Turkel [28] is attributed to be inspired from the ACM. Following initial studies, two more distinct groups of preconditioning methods are developed. The first class of these two algorithms was developed by Choi and Merkle [29] and Weiss and Smith [30]. This method employs temperature as dependent variable instead of entropy. The last class of algorithms was developed by Van Leer [31] which employs a symmetric preconditioner. This preconditioner scales the eigenvalues to obtain a condition number of one which is accepted to be the optimum value for best convergence. References [32] and [33] provides a detailed review of these preconditioning methods.

1.4 Preconditioning for Viscous Flow

Despite the extensive literature on the preconditioning methods for inviscid flows, the studies on the preconditioning of the Navier-Stokes equations are limited in number. In the existing literature, it is observed that the interaction between convective and diffusive terms becomes an important issue both in stability and convergence characteristics of the developed preconditioning algorithms when applied to Navier-Stokes equations.

To identify the effect of viscous diffusion on the inviscid preconditioning matrices, a method is proposed by Venkateswaran et al. [34], [35]. The method introduced relates the performance of the preconditioning scheme to the cell Reynolds number. Dohyung [36] has successfully applied this approach and further developed various preconditioners for the Navier-Stokes equations. Other important studies on this topic includes the researches of Godfrey et al. [37], [38], [39]and Colin et al. [40].

1.5 Present Approach and Objectives

In the present study, a novel preconditioning matrix is developed, validated and its performance is assessed on various flow cases in a wide range of flow speeds including incompressible flows. In contrast to the preconditioning methods developed earlier, in the current approach the conservation of energy equation is preconditioned to enforce the divergence free constraint on the velocity field even at the limiting case of incompressible, zero free-stream Mach number flows. The present approach successfully avoids the major difficulties observed in the low speed flows namely the "cancellation" and the "eigenvalue disparity" problems.

Merkle and Choi [41] removes the "cancellation" problem by their pressure splitting method in which the disturbance pressure is used instead of the total static pressure. In this study, a similar approach is employed. The "cancellation" problem is also observed in the solution of the conservation of energy equation [42], which is resolved by a similar approach. The developed preconditioning method employs a non-dimensionalization similar to the pressure-splitting method for both pressure and total energy.

In the present preconditioning method, the second difficulty namely the “eigenvalue disparity” is solved by the over-relaxation of the time derivative terms. These terms are premultiplied by a novel matrix to enhance the convergence behavior without altering the steady state solution.

The preconditioning method developed in this study is applied both to 2-D [43] and 3-D flows [44] for a wide range of flow speeds. The preconditioned flow solutions are compared against non-preconditioned solutions and the preconditioned solutions available in literature for validation and performance assessment.

1.6 Outline

This thesis work consists of 4 chapters.

Chapter 2 presents the preconditioned flow equations developed and the numerical algorithms employed. This chapter starts with the governing equations, their non-dimensionalization and formulation of the present preconditioning method. The details of the spatial and temporal discretisations based on cell centered finite volume method including the upwind flux formulation, the reconstruction of flow variables at the cell interfaces and the boundary conditions are presented in this chapter.

The 2-D and 3-D flow solutions obtained based on the present formulation are presented and discussed in Chapter 3. Validation studies are performed on channel flow, flow over flat plate and flows over NACA0012 and NACA0008 airfoils. Further studies are performed on flows over Onera M6 wing and DLR-F4 wing-body geometries for performance evaluation.

Finally, the conclusions are drawn and some recommendations for future work are made in Chapter 4.

CHAPTER 2

NUMERICAL METHOD

2.1 Governing Equations

The 2-D planar Navier-Stokes equations in conservative form for compressible viscous flows are given in integral form as

$$\frac{\partial}{\partial t}\int_A \vec{Q}dA + \oint_S (\vec{F_c} - \vec{F_v})dS = 0 \tag{2.1}$$

where $\vec{Q}$, $\vec{F_c}$ and $\vec{F_v}$ are the vector of solution variables, the convective flux and viscous flux vectors respectively.

$$\vec{Q} = \begin{pmatrix} \rho \\ \rho u \\ \rho v \\ \rho e_t \end{pmatrix} \quad , \quad \vec{F_c} = \begin{pmatrix} n_x(\rho u) + n_y(\rho v) \\ n_x(\rho u^2 + p) + n_y(\rho uv) \\ n_x(\rho vu) + n_y(\rho v^2 + p) \\ n_x(u(\rho e_t + p)) + n_y(v(\rho e_t + p)) \end{pmatrix}$$

$$\vec{F_v} = \begin{pmatrix} 0 \\ n_x\tau_{xx} + n_y\tau_{xy} \\ n_x\tau_{yx} + n_y\tau_{yy} \\ n_x\Theta_x + n_y\Theta_y \end{pmatrix} \tag{2.2}$$

Θ term for 2-D formulation becomes;

$$
\begin{aligned}
\Theta_x &= u\tau_{xx} + v\tau_{xy} + k\frac{\partial(T)}{\partial x} \\
\Theta_y &= u\tau_{yx} + v\tau_{yy} + k\frac{\partial(T)}{\partial y}
\end{aligned}
\tag{2.3}
$$

Where the ideal gas equation is:

$$
p = (\gamma - 1)(\rho e_t - \frac{1}{2}\rho(u^2 + v^2)) \tag{2.4}
$$

For Newtonian fluids, with the Stokes hypothesis, the viscous stresses can be reformulated as:

$$
\begin{aligned}
\tau_{xx} &= 2\mu\left(\tfrac{\partial u}{\partial x} - \tfrac{1}{3}\nabla\cdot\vec{v}\right) \\
\tau_{yy} &= 2\mu\left(\tfrac{\partial v}{\partial y} - \tfrac{1}{3}\nabla\cdot\vec{v}\right) \\
\tau_{zz} &= 2\mu\left(\tfrac{\partial w}{\partial z} - \tfrac{1}{3}\nabla\cdot\vec{v}\right) \\
\tau_{xy} &= \tau_{yx} = \mu\left(\tfrac{\partial u}{\partial y} + \tfrac{\partial v}{\partial x}\right) \\
\tau_{xz} &= \tau_{zx} = \mu\left(\tfrac{\partial u}{\partial z} + \tfrac{\partial w}{\partial x}\right) \\
\tau_{yz} &= \tau_{zy} = \mu\left(\tfrac{\partial v}{\partial z} + \tfrac{\partial w}{\partial y}\right)
\end{aligned}
$$

Beside the given conservative form, it is also possible to rewrite the governing equations in various non-conservative forms for different reasons. When 1-D equations are considered, instead of $[\rho, \rho u, \rho e_t]$, other flow variable selections such as $[\rho, u, P]$, $[P, u, T]$, $[\rho, \rho u, T]$ and $[\rho, \rho u, S]$ are equally valid where T and S denotes temperature and entropy respectively. As an example, SIMPLE algorithm employs $[\rho, \rho u, T]$ variables. Although changing independent variables does not change the physical characters, their impact on numerical schemes are important. All primitive variable formulations generate unphysical numerical solutions on discontinuities due to the non-differentiability of their fluxes. On the other hand, the corrective actions taken against this problem result in accuracy losses.

2.1.1 Non-Dimensionalization

Non-dimensionalization is a standard process to reveal the general characteristics and relative importance of different terms of partial differential equations. In this chapter, the non-dimensionalization of 2-D formulation is given in details and the 3-D form is given in Appendix A.

It is possible to observe the already explained "cancellation" and "eigenvalue disparity" problems with the proper non-dimensionalization parameters. Since these two problems are relevant to convective terms only, the Euler equations are employed throughout this section whereas viscous terms are added to the final form of the non-dimensionalized equations set for clarity at the end of the section.

In this study, the following non-dimensionalization is firstly employed.

$$\rho^\star = \frac{\rho}{\rho_\infty} \quad u^\star = \frac{u}{U_\infty} \quad x^\star = \frac{x}{x_r} \quad t^\star = \frac{t u_\infty}{x_r} \quad p^\star = \frac{p}{p_\infty}$$

the non-dimensional conservation of momentum equation in x direction without the viscous terms then becomes:

$$\frac{\partial \rho^\star u^\star}{\partial t^\star} + \frac{\partial(\rho^\star u^{\star 2})}{\partial x^\star} + \left(\frac{p_\infty}{\rho_\infty u_\infty^2}\right)\frac{\partial p^\star}{\partial x^\star} + \frac{\partial(\rho^\star u^\star v^\star)}{\partial y^\star} = 0 \tag{2.5}$$

The term $\left(\frac{p_\infty}{\rho_\infty u_\infty^2}\right)$ is equal to $\frac{1}{\gamma M_\infty^2}$ and as M_∞ goes to zero, this term goes to infinity, which is known as the "cancellation" problem. In a similar manner, the "cancellation" problem still exists even if the velocity is non-dimensionalized with the speed of sound instead. On the other hand, when the pressure is non-dimensionalized with $(\rho_\infty u_\infty^2)$, the "cancellation" problem is observed in the boundary conditions instead of the governing equations. The free-stream pressure boundary condition then becomes $p_\infty = \frac{1}{\gamma M_\infty^2}$.

The "cancellation" problem of the momentum equations are removed by pressure splitting method developed by Merkle and Choi [41], in which the disturbance pressure is employed to eliminate the dominant base pressure.

$$\rho^\star = \frac{\rho}{\rho_\infty} \quad u^\star = \frac{u}{U_\infty} \quad x^\star = \frac{x}{x_r} \quad t^\star = \frac{tu_\infty}{x_r} \quad p^\star = \frac{p - p_\infty}{\rho_\infty U_\infty^2}$$

Now, the inviscid conservation of momentum equation in x direction becomes:

$$\frac{\partial \rho^\star u^\star}{\partial t^\star} + \frac{\partial(\rho^\star u^{\star 2})}{\partial x^\star} + \frac{\partial\left(p^\star + \frac{1}{\gamma M_\infty^2}\right)}{\partial x^\star} + \frac{\partial(\rho^\star u^\star v^\star)}{\partial y^\star} = 0 \tag{2.6}$$

or:

$$\frac{\partial \rho^\star u^\star}{\partial t^\star} + \frac{\partial(\rho^\star u^{\star 2})}{\partial x^\star} + \frac{\partial(p^\star)}{\partial x^\star} + \frac{\partial\left(\frac{1}{\gamma M_\infty^2}\right)}{\partial x^\star} + \frac{\partial(\rho^\star u^\star v^\star)}{\partial y^\star} = 0 \tag{2.7}$$

Since the term $\frac{1}{\gamma M_\infty^2}$ is constant, its spatial derivative drops out. The pressure splitting method also sets the free stream pressure to zero on far field boundary conditions: $\frac{p-p_\infty}{\rho_\infty U_\infty^2} = 0$.

A form of the "cancellation" problem is also observed on the solution of the conservation of energy equation [42], where a similar approach is followed. When the conservation of energy equation is non-dimensionalized with $(\rho_\infty U_\infty^2)$, the far field boundary condition for total energy becomes $0.5 + \frac{1}{\gamma(\gamma-1)M_\infty^2}$. The unbounded growth on free stream total energy value is also observed and solved by again eliminating the problematic mean total energy value. The non-dimensionalization parameter is selected as $(\rho e_t)^\star = \frac{\rho e_t}{\rho_\infty U_\infty^2} - (\rho e_t)_r$ for this purpose where $(\rho e_t)_r = \frac{1}{\gamma(\gamma-1)M_\infty^2}$. This method is not as effective as the splitting method of pressure since the "cancellation" problem still exists in the governing conservation of energy equation despite the boundary conditions as seen in Equation 2.8. It is important to analyze the non-dimensionalized inviscid conservation of energy equation at this point. The equation becomes:

$$\frac{\partial(\rho e_t)}{\partial t} + \frac{\partial(u(\rho e_t + p + \frac{1}{(\gamma-1)M_\infty^2}))}{\partial x} + \frac{\partial(v(\rho e_t + p + \frac{1}{(\gamma-1)M_\infty^2}))}{\partial y} = 0 \tag{2.8}$$

or:

$$\frac{\partial(\rho e_t)}{\partial t} + \frac{\partial(u(\rho e_t + p))}{\partial x} + \frac{\partial(v(\rho e_t + p))}{\partial y} + \frac{\partial(u(\frac{1}{(\gamma-1)M_\infty^2}))}{\partial x} + \frac{\partial(v(\frac{1}{(\gamma-1)M_\infty^2}))}{\partial y} = 0 \tag{2.9}$$

In opposition to the non-dimensionalized conservation of momentum equation shown in Equation 2.7, the last two terms of Equation 2.9 are far from being constant and does not cancel out. On the contrary, they are responsible for establishment of the divergence free velocity field. Their unbounded character is handled with preconditioning method as explained on the following sections.

The final form of the non-dimensional variables and the resulting governing equations become as follows:

$$\rho^\star = \frac{\rho}{\rho_\infty} \quad u^\star = \frac{u}{U_\infty} \quad p^\star = \frac{p}{\rho_\infty U_\infty^2} - p_r \quad (\rho e_t)^\star = \frac{\rho e_t}{\rho_\infty U_\infty^2} - (\rho e_t)_r$$
$$x^\star = \frac{x}{x_r} \quad t^\star = \frac{t u_\infty}{x_r}$$

The reference values of p_r and $(\rho e_t)_r$ are chosen as $\frac{1}{\gamma M_\infty^2}$ and $\frac{1}{\gamma(\gamma-1)M_\infty^2}$.

The final form of non-dimensional 2-D Navier-Stokes equations is obtained with the addition of viscous terms;

$$\frac{\partial}{\partial t}\int_A \vec{Q}dA + \oint_S (\vec{F_c} - \vec{F_v})dS = 0 \tag{2.10}$$

where,

$$\vec{Q} = \begin{pmatrix} \rho \\ \rho u \\ \rho v \\ \rho e_t \end{pmatrix}$$

$$\vec{F_c} = \begin{pmatrix} n_x(\rho u) + n_y(\rho v) \\ n_x(\rho u^2 + p) + n_y(\rho uv) \\ n_x(\rho vu) + n_y(\rho v^2 + p) \\ n_x(u(\rho e_t + p + \frac{1}{(\gamma-1)M_\infty^2})) + n_y(v(\rho e_t + p + \frac{1}{(\gamma-1)M_\infty^2})) \end{pmatrix}$$

$$\vec{F_v} = \begin{pmatrix} 0 \\ n_x\tau_{xx} + n_y\tau_{xy} \\ n_x\tau_{yx} + n_y\tau_{yy} \\ n_x\Theta_x + n_y\Theta_y \end{pmatrix} \tag{2.11}$$

The non-dimensional viscous stresses, work of viscous stresses and the heat conduction can be formulated as:

$$\begin{aligned} \tau_{xx} &= \frac{2}{Re}\left(\frac{\partial u}{\partial x} - \frac{1}{3}\nabla\cdot\vec{v}\right) \\ \tau_{yy} &= \frac{2}{Re}\left(\frac{\partial v}{\partial y} - \frac{1}{3}\nabla\cdot\vec{v}\right) \\ \tau_{xy} = \tau_{yx} &= \frac{1}{Re}\left(\frac{\partial u}{\partial y} + \frac{\partial v}{\partial x}\right) \\ \Theta_x &= u\tau_{xx} + v\tau_{xy} + k\frac{\partial(T)}{\partial x} \\ \Theta_y &= u\tau_{yx} + v\tau_{yy} + k\frac{\partial(T)}{\partial y} \end{aligned} \tag{2.12}$$

where,

$$k = \frac{\gamma}{RePr} \tag{2.13}$$

The asterisks have been dropped for notational convenience.

The corresponding non-dimensional free-stream conditions become:

$$\rho_\infty = 1 \quad u_\infty = 1 \quad p_\infty = 0 \quad (\rho e_t)_\infty = 0.5$$

2.1.2 Preconditioning

It is important to note that, in the non-dimensional formulation given on Equation 2.10 and Equation A.1, the free-stream conditions and the conservation of momentum equations do not contain any singularity. However, the singularity problem still exists in the conservation of energy equation for zero free-stream Mach number flows. This singularity is next removed by introducing a new preconditioning matrix described below.

The eigenvalues of the non-dimensional set of equations 2.10 are:

$$\lambda_1 = u - c \quad \lambda_2 = u \quad \lambda_3 = u \quad \lambda_4 = u + c$$

where the modified speed of sound, c is given by

$$c = \sqrt{\frac{\gamma p}{\rho} + \frac{1}{\rho M_\infty^2}}$$

It should also be noted that as M_∞ goes to zero, the $u+c$ and $u-c$ eigenvalues go to $\pm\infty$ as in the case of original formulation.

The novel formulation is developed by first relaxing the time derivative terms in both the conservation of mass and energy equations. It is achieved simply by dividing them with M_∞^2 or multiplying the remaining terms by M_∞^2.

$$\begin{aligned}
\frac{\partial \rho}{\partial t} + M_\infty^2 \frac{\partial(\rho u)}{\partial x} + M_\infty^2 \frac{\partial(\rho v)}{\partial y} &= 0 \\
\frac{\partial(\rho u)}{\partial t} + \frac{\partial(\rho u^2 + p)}{\partial x} + \frac{\partial(\rho u v)}{\partial y} &= \frac{\partial \tau_{xx}}{\partial x} + \frac{\partial \tau_{xy}}{\partial y} \\
\frac{\partial(\rho v)}{\partial t} + \frac{\partial(\rho u v)}{\partial x} + \frac{\partial(\rho v^2 + p)}{\partial y} &= \frac{\partial \tau_{yx}}{\partial x} + \frac{\partial \tau_{yy}}{\partial y} \\
\frac{\partial(\rho e_t)}{\partial t} + M_\infty^2 \frac{\partial(u(\rho e_t + p + \frac{1}{M_\infty^2(\gamma-1)}))}{\partial x} + M_\infty^2 \frac{\partial(v(\rho e_t + p + \frac{1}{M_\infty^2(\gamma-1)}))}{\partial y} & \\
= M_\infty^2 \frac{\partial \Theta_x}{\partial x} + M_\infty^2 \frac{\partial \Theta_y}{\partial y} &
\end{aligned} \tag{2.14}$$

At the limiting case of zero free stream Mach number and no heat exchange from boundaries, the equation set becomes:

$$
\begin{gathered}
\frac{\partial \rho}{\partial t} = 0 \\
\frac{\partial(\rho u)}{\partial t} + \frac{\partial(\rho u^2 + p)}{\partial x} + \frac{\partial(\rho uv)}{\partial y} = \frac{1}{Re}\left(\frac{\partial^2 u}{\partial x^2} + \frac{\partial^2 u}{\partial x^2}\right) \\
\frac{\partial(\rho v)}{\partial t} + \frac{\partial(\rho uv)}{\partial x} + \frac{\partial(\rho v^2 + p)}{\partial y} = \frac{1}{Re}\left(\frac{\partial^2 v}{\partial x^2} + \frac{\partial^2 v}{\partial x^2}\right) \\
\frac{\partial(\rho e_t)}{\partial t} + \frac{1}{(\gamma - 1)}\frac{\partial u}{\partial x} + \frac{1}{(\gamma - 1)}\frac{\partial v}{\partial y} = 0
\end{gathered} \tag{2.15}
$$

The relaxed and preconditioned conservation of mass equation diminishes for incompressible flows. Yet, the conservation of energy equation becomes bounded and provides the divergence free velocity constraint. However, the eigenvalues and eigenvectors of the equations set given above are rather complex in terms of equation length when compared with the ACM formulation. Recovering the ACM equation at the incompressibility limit is intended to overcome this difficulty.

The preconditioned conservation of energy equation given in Equation 2.15 and the modified conservation of mass equation of the ACM method are very similar. The exception is that the time rate of change of total energy is considered in the former instead of the artificial density or pressure in the latter. The formulation of original ACM is given below for comparison.

$$
\begin{gathered}
\frac{\partial P}{\partial t} + \frac{\partial u}{\partial x} + \frac{\partial v}{\partial y} = 0 \\
\frac{\partial u}{\partial t} + \frac{\partial(u^2 + p)}{\partial x} + \frac{\partial(uv)}{\partial y} = \frac{1}{Re}\left(\frac{\partial^2 u}{\partial x^2} + \frac{\partial^2 u}{\partial x^2}\right) \\
\frac{\partial v}{\partial t} + \frac{\partial(uv)}{\partial x} + \frac{\partial(v^2 + p)}{\partial y} = \frac{1}{Re}\left(\frac{\partial^2 v}{\partial x^2} + \frac{\partial^2 v}{\partial x^2}\right)
\end{gathered} \tag{2.16}
$$

In the present formulation, the relation between pressure and the total energy is obtained through the ideal gas equation. Its differentiation with respect to time for incompressible flows provides the necessary equation to obtain the ACM formulation exactly at zero free stream Mach number with the present preconditioning scheme.

$$\frac{1}{(\gamma-1)}\frac{\partial p}{\partial t} = (\frac{\partial(\rho e_t)}{\partial t} - u\frac{\partial(\rho u)}{\partial t} - v\frac{\partial(\rho v)}{\partial t}) \tag{2.17}$$

When Equation 2.17 is substituted into Equation 2.14, the modified conservation of mass equation of the original ACM formulation can be recovered by subtracting the $u\frac{\partial(\rho u)}{\partial t}$ and $v\frac{\partial(\rho v)}{\partial t}$ terms at zero free stream Mach number:

$$\begin{gathered}
\frac{\partial \rho}{\partial t} = 0 \\
\frac{\partial(\rho u)}{\partial t} + \frac{\partial(\rho u^2+p)}{\partial x} + \frac{\partial(\rho uv)}{\partial y} = \frac{1}{Re}\left(\frac{\partial^2 u}{\partial x^2} + \frac{\partial^2 u}{\partial x^2}\right) \\
\frac{\partial(\rho v)}{\partial t} + \frac{\partial(\rho uv)}{\partial x} + \frac{\partial(\rho v^2+p)}{\partial y} = \frac{1}{Re}\left(\frac{\partial^2 v}{\partial x^2} + \frac{\partial^2 v}{\partial x^2}\right) \\
\underbrace{\frac{\partial(\rho e_t)}{\partial t} - u\frac{\partial(\rho u)}{\partial t} - v\frac{\partial(\rho v)}{\partial t}}_{\frac{1}{(\gamma-1)}\frac{\partial p}{\partial t}} + \frac{1}{(\gamma-1)}\frac{\partial u}{\partial x} + \frac{1}{(\gamma-1)}\frac{\partial v}{\partial y} = 0
\end{gathered} \tag{2.18}$$

Although the addition/subtraction of such unsteady terms affects the transient behavior of the solution, once the solution converges to a steady-state, the divergence free velocity field is satisfied, which is the general character of the ACM and all other preconditioning schemes.

The major solution method used to restore the time accurate character of governing equations is the dual time stepping method [46]. In this method, a steady problem is solved in each physical time step by addition of a pseudo time term. Dual time stepping is widely used with preconditioning methods in the literature [47], [48], [49]. All the test cases selected in this study are steady state and dual time stepping method is not employed.

The final form of the preconditioned system of Euler equations now becomes:

$$
\begin{aligned}
\frac{\partial \rho}{\partial t} + M_\infty^2 \frac{\partial(\rho u)}{\partial x} + M_\infty^2 \frac{\partial(\rho v)}{\partial y} &= 0 \\
\frac{\partial(\rho u)}{\partial t} + \frac{\partial(\rho u^2 + p)}{\partial x} + \frac{\partial(\rho u v)}{\partial y} &= \frac{\partial \tau_{xx}}{\partial x} + \frac{\partial \tau_{xy}}{\partial y} \\
\frac{\partial(\rho v)}{\partial t} + \frac{\partial(\rho u v)}{\partial x} + \frac{\partial(\rho v^2 + p)}{\partial y} &= \frac{\partial \tau_{yx}}{\partial x} + \frac{\partial \tau_{yy}}{\partial y} \\
\frac{\partial(\rho e_t)}{\partial t} - (1 - M_\infty^2) u \frac{\partial(\rho u)}{\partial t} - (1 - M_\infty^2) v \frac{\partial(\rho v)}{\partial t} &+ \frac{\partial(u(M_\infty^2 \rho e_t + M_\infty^2 p + \frac{1}{(\gamma-1)}))}{\partial x} \\
+ \frac{\partial(v(M_\infty^2 \rho e_t + M_\infty^2 p + \frac{1}{(\gamma-1)}))}{\partial y} &= M_\infty^2 \frac{\partial \Theta_x}{\partial x} + M_\infty^2 \frac{\partial \Theta_y}{\partial y} \\
-(1 - M_\infty^2) u \left(\frac{\partial \tau_{xx}}{\partial x} + \frac{\partial \tau_{xy}}{\partial y} \right) &- (1 - M_\infty^2) v \left(\frac{\partial \tau_{yx}}{\partial x} + \frac{\partial \tau_{yy}}{\partial y} \right) \qquad (2.19)
\end{aligned}
$$

The equation set given above can also be expressed in matrix form:

$$
\frac{\partial \vec{Q}}{\partial t} + \Gamma \left(\frac{\partial(\vec{E}_c - \vec{E}_v)}{\partial x} + \frac{\partial(\vec{F}_c - \vec{F}_v)}{\partial y} \right) = 0 \qquad (2.20)
$$

where

$$
\vec{Q} = \begin{pmatrix} \rho \\ \rho u \\ \rho v \\ \rho e \end{pmatrix} , \; \vec{E}_c = \begin{pmatrix} \rho u \\ \rho u^2 + p \\ \rho u v \\ u \left(\rho e + p + \frac{1}{(\gamma-1) M_\infty^2} \right) \end{pmatrix} , \; \vec{F}_c = \begin{pmatrix} \rho v \\ \rho u v \\ \rho v^2 + p \\ v \left(\rho e + p + \frac{1}{(\gamma-1) M_\infty^2} \right) \end{pmatrix}
$$

$$
\vec{E}_v = \begin{pmatrix} 0 \\ \tau_{xx} \\ \tau_{yx} \\ \Theta_x \end{pmatrix} , \; \vec{F}_v = \begin{pmatrix} 0 \\ \tau_{yx} \\ \tau_{yy} \\ \Theta_y \end{pmatrix}
$$

and Γ is the Mach uniform preconditioning matrix:

$$\Gamma = \begin{bmatrix} M_\infty^2 & 0 & 0 & 0 \\ 0 & 1 & 0 & 0 \\ 0 & 0 & 1 & 0 \\ 0 & (1-M_\infty^2)u & (1-M_\infty^2)v & M_\infty^2 \end{bmatrix}$$

The flux jacobian matrix, J, and the eigenvalues of the preconditioned 2-D system in the orthonormal basis are obtained as:

$$J = \begin{pmatrix} 0 & M_\infty^2 & 0 & 0 \\ \frac{(\gamma-1)q}{2} - u'^2 & (3-\gamma)u' & -(\gamma-1)v' & (\gamma-1) \\ -u'v' & v' & u' & 0 \\ \frac{u'(Aq/2-B)}{(\gamma-1)} & \frac{B-(A+(\gamma-1))u'^2}{(\gamma-1)} - \frac{(M_\infty^2-2)q}{2} & -Hu'v' & (H+1)u' \end{pmatrix}$$

$$\lambda_1 = u' \quad \lambda_2 = u'M_\infty^2 \quad \lambda_3 = u' - c \quad \lambda_4 = u' + c$$

where u' and v' represents the velocity components normal and tangential to the edge where the fluxes are evaluated. The modified speed of sound, c, and the terms q, A, B and H are given by

$$\begin{aligned} c &= \sqrt{\frac{\gamma p M_\infty^2 + 1}{\rho} + (1-M_\infty^2)u'^2} \\ q &= u'^2 + v'^2 \\ A &= \gamma^2 + (M_\infty^2 - 4)\gamma + 3 - M_\infty^2 \\ B &= c^2 + (M_\infty^2 - 1)u'^2 \\ H &= (\gamma - 2 + M_\infty^2) \end{aligned} \tag{2.21}$$

The 3-D version of the present preconditioning method is also developed with the same methodology and given in Appendix B.

The present preconditioning method recovers the ACM at the limiting case of incompressible flows, which differentiates it from the other well-known preconditioning methods [50], [51]. It should be noted that the modified speed of sound is bounded for $-1 \leq M_\infty < 1$, and has a value of $\sqrt{\frac{1}{\rho} + \frac{u^2}{\rho^2}}$ at $M_\infty = 0$.

The condition number of the present formulation becomes $|u + c| / |u - c| \approx 5.83$ for incompressible flows which is the same as that of the ACM with $\delta = 1$ where δ is the ACM parameter. This condition number value is approximately twice the value of the Choi-Merkle preconditioner[29]. In the ACM, the condition number can be reduced to approximately 2.6 when δ is defined as proportional to flow velocity [52]. A similar approach can also be considered in the present formulation in order to improve the convergence rate.

The variation of condition number of the present formulation and non-preconditioned formulation with Mach number is compared in Figure 2.1.

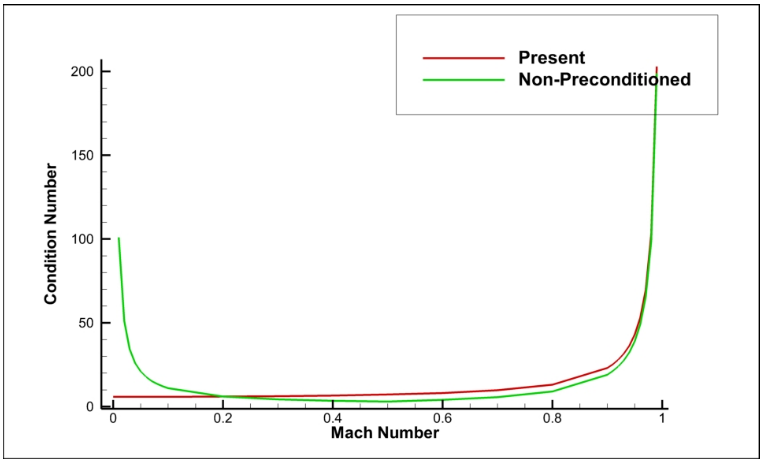

Figure 2.1: Variation of condition number with Mach number

It is observed from Figure 2.1 that the increase in condition number, as approaching to $M_\infty = 0$, is prevented with current preconditioning approach. An almost uniform condition number is achieved for low speed regime.

2.2 Flow Solver

The developed Mach uniform preconditioner is implemented in 2-D and 3-D in-house flow solvers. A compressible Navier-Stokes solver is developed as the base solver to be used on 2-D test cases. On the other hand, instead of developing a new 3-D flow solver, a simplified version of an already validated in-house code named as HYP3D is employed [53], [54]. Since the main objective of this study is to validate the performance of the present new preconditioning method, relatively simple temporal discretization schemes such as Runge-Kutta and Point Gauss Seidel methods are selected.

As opposed to the flow solvers based on SIMPLE algorithm, the preconditioning methods preserves the general structure of the compressible flow equations. Solution algorithms for the convergence acceleration such as GMRES method [55], [56] or multigrid algorithms [57], [58] can easily be employed to the present formulation.

The 2-D and 3-D flow solvers are both based on cell centered finite volume discretization schemes. These solvers can use structured and unstructured mesh types. The 2-D quadrilateral grids are generated with an in-house hyperbolic grid generator [59], the 3-D Onera M6 test case mesh is generated with open source mesh generator enGrid and DLR-F4 test case mesh is generated with commercial grid generation software GAMBIT^{TM}.

The details of the employed schemes are given on the following subsections.

2.2.1 Spatial Discretization

In this study, separate discretization in space and time which is named as method of lines [60] is employed. This method uses grids to approximate the spatial derivatives of the flow quantities and in a further step, the equations are advanced in time with the selected temporal discretization method. Since the governing preconditioned equations are false transient, advancement in time corresponds to an iterative process to obtain steady-state solution.

Both of the developed 2-D and 3-D flow solvers employ finite volume method where integral form of the conservation laws are used.

$$\frac{\partial}{\partial t}\int_V \vec{Q}dV + \oint_S (\vec{F_c} - \vec{F_v})dS = 0$$

In cell centered finite volume methods, the flow variables are stored at the cell centers and surface integrals of fluxes are approximated by the sum of the fluxes crossing individual faces of the control volumes as shown in Figure 2.2.

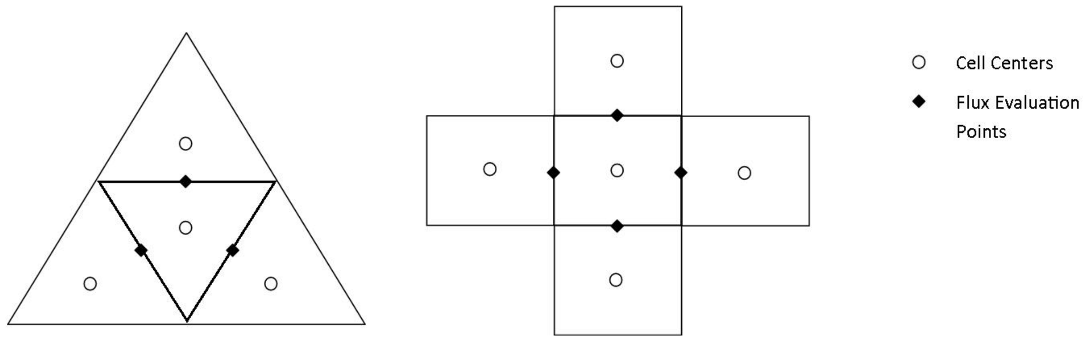

Figure 2.2: Cell centered finite volume

For planar control volume surfaces, the closed path integral can be represented as summation and the resulting equation becomes:

$$\frac{\partial \vec{Q}}{\partial t} = -\frac{1}{V}\sum_{i=1}^{n}(\vec{F}_c - \vec{F}_v)\Delta S$$

The spatial discretization process consists of the methods used for evaluation of these terms and different approaches are needed for convective and diffusive fluxes. These employed methods are explained on the following subsections.

2.2.1.1 Convective Fluxes

The methods used for flux evaluation significantly influence both the stability and the accuracy of the resulting solutions. The convective part of the Navier-Stokes equations have an hyperbolic character and evaluation of these fluxes at control volume faces needs special treatment when compared with diffusive fluxes. The simple average of fluxes computed from the cell center values of either side does not result in stable schemes. Two of the mostly used approaches for this problem are addition of artificial dissipation terms [61] and upwinding methods.

In general, artificial dissipation methods are easy to implement and computationally inexpensive when compared with upwinding methods. These methods mostly consist of a high order dissipation term for the whole domain and a low order term for regions with high gradients or discontinuities such as shockwaves. The major concern about the artificial dissipation method is to predict the user controlled and problem dependent inputs. The magnitude of user defined dissipation coefficients should be enough to suppress unphysical oscillations and should not deteriorate the solution accuracy at the same time.

As the second method, upwinding schemes has an inherent dissipation character and does not need any user specified inputs. Flux Difference Splitting(FDS) and Flux Vector Splitting(FVS) Methods are the major categories of upwinding methods. The details of these methods are analyzed in [24] for the ACM formulation but it is important to state that, since the current preconditioning formulation recovers the ACM at incompressibility limit, it does not have the homogeneity property either. All FVS methods rely on this property and are not applicable to the current formulation.

Roe approximate Riemann solver is employed for the convective fluxes in this study and evaluated with the general formula:

$$\frac{1}{2}\left(\vec{F}_L + \vec{F}_R - R\left|\lambda\right| R^{-1}\Delta\vec{Q}\right) \tag{2.22}$$

where F_L and F_R are left and right state fluxes. λ and R are eigenvalues and the right eigenvectors of the preconditioned jacobian matrix formed by the Roe averaged flow variables respectively. The right eigenvectors matrix and its inverse are obtained by using the commercial symbolic algebra software MAPLE [62] for both 2-D and 3-D formulations. The 2-D version is given below in the orthonormal basis and the 3-D form is given in Appendix B. u' and v' represents normal and tangential velocity components.

$$\lambda = \begin{pmatrix} u' \\ u' M_\infty^2 \\ u' - c \\ u' + c \end{pmatrix}$$

$$
R = \begin{pmatrix} 0 & 1 & M_\infty^2 & M_\infty^2 \\ 0 & u' & u' - c & u' + c \\ 1 & 0 & \frac{v'(u'(M_\infty^2-1)+c)}{c} & -\frac{v'(u'(M_\infty^2-1)-c)}{c} \\ v' & \frac{(u'^2-v'^2)}{2} + \frac{(M_\infty^2-1)u'^2}{(\gamma-1)} & D - E & D + E \end{pmatrix}
$$

$$
R^{-1} = \begin{pmatrix} -\frac{v'(\gamma-1)q}{2c^2} & \frac{v'u'H}{c^2} & \frac{(\gamma-1)v'^2+c^2}{c^2} & -\frac{(\gamma-1)v'}{c^2} \\ \frac{M_\infty^2(\gamma-1)q-2(M_\infty^2-1)u'^2-2c^2}{2FG} & -\frac{u'(\gamma-1)M_\infty^2}{FG} & -\frac{M_\infty^2(\gamma-1)v'}{FG} & \frac{M_\infty^2(\gamma-1)}{FG} \\ \frac{(\gamma-1)q+2u'c}{4Fc} & -\frac{u'H+c}{2Fc} & -\frac{(\gamma-1)v'}{2Fc} & \frac{(\gamma-1)}{2Fc} \\ -\frac{(\gamma-1)q-2u'c}{4Gc} & \frac{u'H-c}{2Gc} & \frac{(\gamma-1)v'}{2Gc} & -\frac{(\gamma-1)}{2Gc} \end{pmatrix} \tag{2.23}
$$

where c, q and H are defined in Equation 2.21 and

$$
\begin{aligned}
D &= \frac{(M_\infty^2-1)u'^2+c^2}{(\gamma-1)} - \frac{(M_\infty^2-2)q}{2} \\
E &= u'c - \frac{(M_\infty^2-1)u'v'^2}{c} \\
F &= (M_\infty^2 - 1)u' + c \\
G &= (M_\infty^2 - 1)u' - c
\end{aligned} \tag{2.24}
$$

2.2.1.2 Viscous Fluxes

In the discretization of viscous fluxes, the first order derivatives of flow variables on edges/surfaces are needed to be evaluated beside the flow variables. For this purpose, "element-based gradients" and "average of gradients" methods can be used.

Element-based gradients method rely on the construction of auxiliary control volumes where the centers of the new generated volumes coincide with the points where gradients should be evaluated. The data structure should be extended in these methods and according to the implementation strategy, memory and/or number of operations cost increases.

As the second method, average of gradients is particularly attractive if gradients in each control volume is already computed. Also, no additional storage of geometrical coefficients are needed. The major drawback of this method is its extending the stencil of computational nodes.

In this study the average of gradients method is implemented and used where the averaging formula is given below.

$$\overline{\nabla Q_{ij}} = \frac{1}{2}\left(\nabla Q_i + \nabla Q_j\right) \tag{2.25}$$

It should be noted that, the averaging process given above is compatible with the diffusive character of the viscous fluxes and does not introduce any stability issues while preserving the second order spatial accuracy.

2.2.2 Flow Variable Reconstruction at the Cell Interfaces

The left and right state fluxes are used on evaluation of the fluxes on cell interfaces as given in Equation 2.22. These fluxes should be evaluated with adjacent flow variables on either side of the interface. A sample cell interface is shown in Figure 2.3.

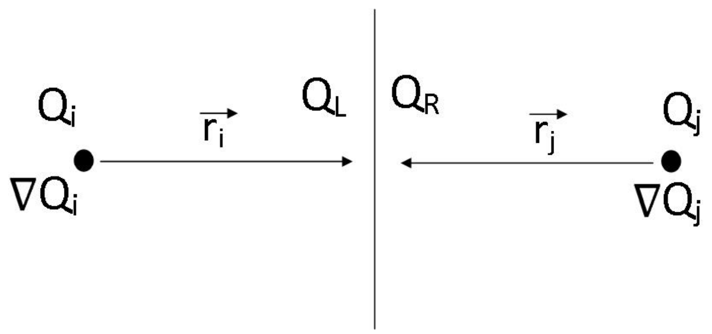

Figure 2.3: Representative edge for flow variable reconstruction

The simplest variable reconstruction method is obtained by taking left and right state variables as equal to the cell center values of the corresponding sides which results in first order reconstruction for convective fluxes and second order reconstruction on viscous fluxes. Since first order schemes are diffusive, no extra prevention is needed for evaluation of convective terms on discontinuities such as shock waves.

Higher order schemes are the main solution methods to reduce the numerical diffusion and to increase the spatial accuracy of solutions in the literature. In order to obtain these schemes, extra information is used by increasing the stencil length. There are various fixed and variable stencil high order schemes in the literature but by far the most widely used scheme on unstructured grids is the gradient based second order scheme. This method is employed on the developed 2-D flow solver where the formulas are:

$$
\begin{aligned}
Q_L &= Q_i + \nabla Q_i \cdot \vec{r}_i \\
Q_R &= Q_j + \nabla Q_j \cdot \vec{r}_j
\end{aligned}
$$

The gradients of flow variables ∇Q are evaluated at the cell centers again with the finite volume methodology. When Green's theorem is appplied, the resulting gradient evaluation formula becomes:

$$\nabla Q = \frac{1}{V} \oint_S Q dS \tag{2.26}$$

For planar integration surfaces, Equation 2.26 can be written in summation form as:

$$\nabla Q = \frac{1}{V} \sum_{i=1}^{i_{max}} Q_i \Delta S \tag{2.27}$$

In Equation 2.27 the reconstructed flow variables on cell faces Q_i are taken as arithmetic averages of cell center values of both sides.

Usage of high resolution schemes on solutions results in spurious oscillations on the flow field especially near discontinuities. A sufficient condition to avoid these wiggles is not to form new local extremities during flow variables reconstruction process. Slope limiters are one of the methods used for this purpose. The slope limiter of Barth and Jespersen [63] is employed in the second order reconstruction of flow variables to suppress stability problems on cases with shock waves. The limited reconstruction formula for the left state is shown as an example.

$$Q_L = Q_i + \Phi_i \nabla Q_i \cdot \vec{r}_i \tag{2.28}$$

where:

$$\Phi_i = \begin{cases} \min\left(1, \frac{\delta Q_i^{max}}{Q_{LR}-Q_i}\right), & \text{if } Q_L - Q_i > 0 \\ \min\left(1, \frac{\delta Q_i^{min}}{Q_{LR}-Q_i}\right), & \text{if } Q_L - Q_i < 0 \\ 1, & \text{if } Q_L - Q_i = 0 \end{cases} \tag{2.29}$$

The δQ_i^{max} and δQ_i^{min} values are respectively the positive and negative differences between the neighbors and the volume where the fluxes to be calculated. Q_{LR} corresponds to the unconstrained reconstructed values.

2.2.3 Boundary Conditions

Boundary conditions play a significant role both on the convergence characteristics and the accuracy of flow solvers. Beside representing the physical conditions, one of the major goals of boundary conditions is to obtain non-reflectivity character. In compressible formulations, Method of Characteristics based boundary conditions are employed for this purpose and the obtained results work far more better than the reflecting boundary conditions [64], [65]. On the other hand, changing eigensystem of the governing equations also changes the characteristic variables [65], [66].

The characteristic form of the 1-D preconditioned system of equations can be represented as given below.

$$\frac{\partial \vec{W}}{\partial t} = \lambda \frac{\partial \vec{W}}{\partial x}$$

The characteristic variables $\vec{W}$ can be calculated with the formula:

$$\vec{W} = R^{-1}\vec{Q}$$

The resulting characteristic variables of the proposed formulation are found to be too complex to code in terms of length. Derivation of non-reflecting boundary conditions for the new preconditioned system of equations is a comprehensive work and is not included in this study.

Between the reflective and non-reflecting boundary conditions, there are various different formulations which have reduced reflectivity. The effectiveness of these methods are observed to be sensitive to the governing equations. In this study, reflective far-field boundary conditions are selected and employed to eliminate the unforeseeable effects of reflectivity reduction efforts on convergence rate of different governing equations sets.

For subsonic external flows, the following standard boundary conditions, which are also employed in Artificial Compressibility Method, are implemented:

$$\begin{array}{llll}
\rho = \rho_\infty & \rho\vec{V} = (\rho\vec{V})_\infty & P = P_{ext} & \text{for inflow} \\
\rho = \rho_{ext} & \rho\vec{V} = (\rho\vec{V})_{ext} & P = P_\infty & \text{for outflow} \\
\rho = \rho_{ext} & \rho V_n = 0 & P = P_{ext} & \text{for inviscid wall} \\
\rho = \rho_{ext} & \rho\vec{V} = 0 & P = P_{ext} & \text{for viscous wall}
\end{array}$$

where ∞ and ext correspond to free-stream values and extrapolated values from the solution domain respectively.

It should be noted that for high subsonic flows, these boundary conditions results in significant variations on the inflow total energy, especially when high levels of disturbances interact with near-field boundaries. For such cases, including channel flows, the entropy and the stagnation enthalpy at the inflow and the pressure at the outflow are taken as the free-stream values. The remaining variables are extrapolated from the interior flow solution.

For supersonic cases, all of the flow variables are taken as the free-stream values at the inflow and extrapolated from the interior solution at the outflow.

2.2.4 Temporal Discretization

When advancement in time is separated from the spatial discretization, the governing set of equations can be represented in vectorial form as:

$$\frac{\partial \vec{Q}}{\partial t} = \vec{R} \tag{2.30}$$

There are various different methods for disretization of this equation set in the literature with different performance and complexity levels. Although these methods can be grouped in two main categories as explicit and implicit schemes, significant variations can also be observed within these categories.

The evaluation method of the right hand side residual term is the main difference between implicit and explicit schemes. While the residual term is evaluated at the previous time level in explicit schemes, the implicit schemes use the new time level which results in non-linearity. A linearization process is needed and Taylor Series expansion is employed for this purpose on implicit schemes.

$$R^{\vec{n+1}} \approx \vec{R^n} + \left(\frac{\partial \vec{R}}{\partial Q}\right) \Delta Q \tag{2.31}$$

The $\left(\frac{\partial \vec{R}}{\partial Q}\right)$ term is named as Flux Jacobian and contains terms for all the cells in discretization stencil.

The developed 2-D flow solver utilizes widely used Point Gauss Seidel method due to its relatively high performance and low numerical complexity. The off-diagonal terms are neglected in this method but the diagonal terms assure extended stability range.

On the other hand, explicit schemes are easier than the implicit ones. The most basic explicit scheme can be obtained by a forward difference in time and can be represented as:

$$\Delta\vec{Q}^n = \frac{\Delta t}{V}\vec{R}^n \tag{2.32}$$

In this formulation the residual term is evaluated at the previous time level and a single-stage scheme is obtained. In literature, there are also multi-stage schemes where the solution is advanced in time with several stages. At each stage, residuals are weighted with coefficients in these methods. Inner trial steps reduce the lower-order error terms and increase temporal accuracy in these multi-stage schemes. Runge Kutta schemes [67] are the most popular of these methods and three stage Runge-Kutta time stepping scheme is employed on the 3-D flow solutions. Since the preconditioned formulation is false transient, all the test cases are selected from steady flows and temporal accuracy is not relevant but Runge Kutta method also extends the stable time step range and allows faster convergence.

2.2.5 High Performance Computing

The ever growing demand on increased modeling complexity and reduced computation time results in turning towards high performance computing (HPC) in CFD simulations. HPC is the use of parallel processing methods to expand the computational resources. When CFD is concerned, multi-core processors combined with centralization is the core trend. It becomes possible to simulate large scale problems in reasonable times with these clusters.

Beyond hardware, the software should also be suitable for parallel computations. The 3-D flow solver employed in this study (HYP3D) has the capability of parallel computation in its base form. The developed preconditioning formulation does not influence the relevant parts of the original code and any extra effort on parallellization is not needed.

HYP3D flow solver employs Metis graph partitioning method [68] and Parallel Virtual Machine (PVM) [69] libraries. METIS is one of the most efficient tools/libraries for partitioning. This library is used for grid partitioning where it is based on multilevel recursive-bisection, multilevel k-way and multi-constraint partitioning schemes.

To ensure the connectivity between the grid partitions in solution domain, data transfer on partition interfaces are needed. PVM is the selected library for this purpose which allows message-passing, task and resource management and fault notification on heterogeneous computers network. These tasks can be performed on both shared and local memory networks.

The 3-D solutions presented in this study are conducted on HPC-Poyraz cluster of METU Center for Wind Energy - High Performance Computing Laboratory which is an education/research oriented PC cluster. HPC-Poyraz cluster consists of:

- 1 server node :
  - 2 Intel Xeon 1.6 GHz CPUs with 4 cores and 4MB cache memory per CPU
  - 32GB DDR3 with 1333 MHz 8GB DIMM Memory
- 8 nodes :
  - 4 AMD Opteron 6276 2.3 GHz CPUs with 16 cores and 32MB cache memory per CPU at each node
  - 256 GB DDR3 with 1333 MHz 8 GB DIMM Memory per node

CHAPTER 3

RESULTS AND DISCUSSION

The developed all speed preconditioning method is validated on 2-D and 3-D flow test cases. Except the supersonic flows, the preconditioner is activated in all solutions. The unpreconditioned solutions are also obtained for comparison. Since two different flow solvers are utilized in 2-D and 3-D solutions, their validation and performance evaluation studies are presented separately in the following two subsections.

3.1 Two Dimensional Cases

3.1.1 Inviscid Flow Cases

All newly proposed preconditioning formulations are firstly validated on inviscid flow cases since the major problems are mostly originated from the convective terms. In consistence with the literature, two widely used test cases are selected and studied extensively for validation and performance evaluation of the proposed formulation. The 2-D inviscid test cases start with the flows in a channel flow with a circular bump. As the second 2-D inviscid case, flow over a NACA0012 airfoil profile is studied. The internal bump flow cases are considered as validation cases for accuracy and the stability of the developed flow solver. Inviscid external flow over airfoil is used as 2-D performance evaluation test case where the interaction with outer boundaries are insignificant when compared with internal flow cases.

3.1.1.1 Flow in a Channel with a Circular Bump

Three different inflow Mach numbers, 0.01, 0.675 and 1.40 are considered in this channel flow case. The circular bump height is taken as 10 percent for the subsonic and transonic flow cases, and 4 percent for the supersonic flow case in accordance with the reference study performed by Ni [70]. The computational grid which is of 252x54 size is employed in both cases as shown in Figure 3.1.

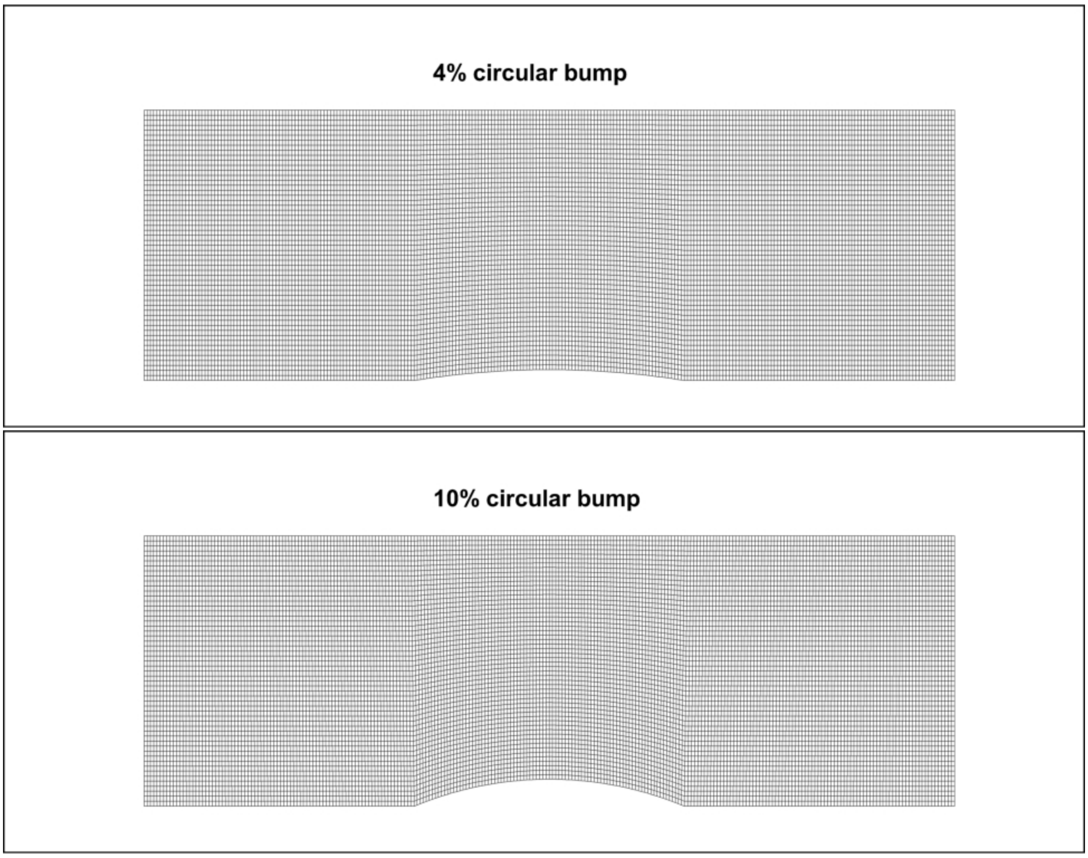

Figure 3.1: Computational grids employed for channel flows with circular bumps

The pressure coefficient distributions in the channel for different Mach numbers are computed and shown in Figure 3.2 as flood contour for visualization. As seen in these figures, the shocks and the shock reflections in the transonic and the supersonic flow cases are resolved sharply. Also no wiggles are observed on the low subsonic flow case.

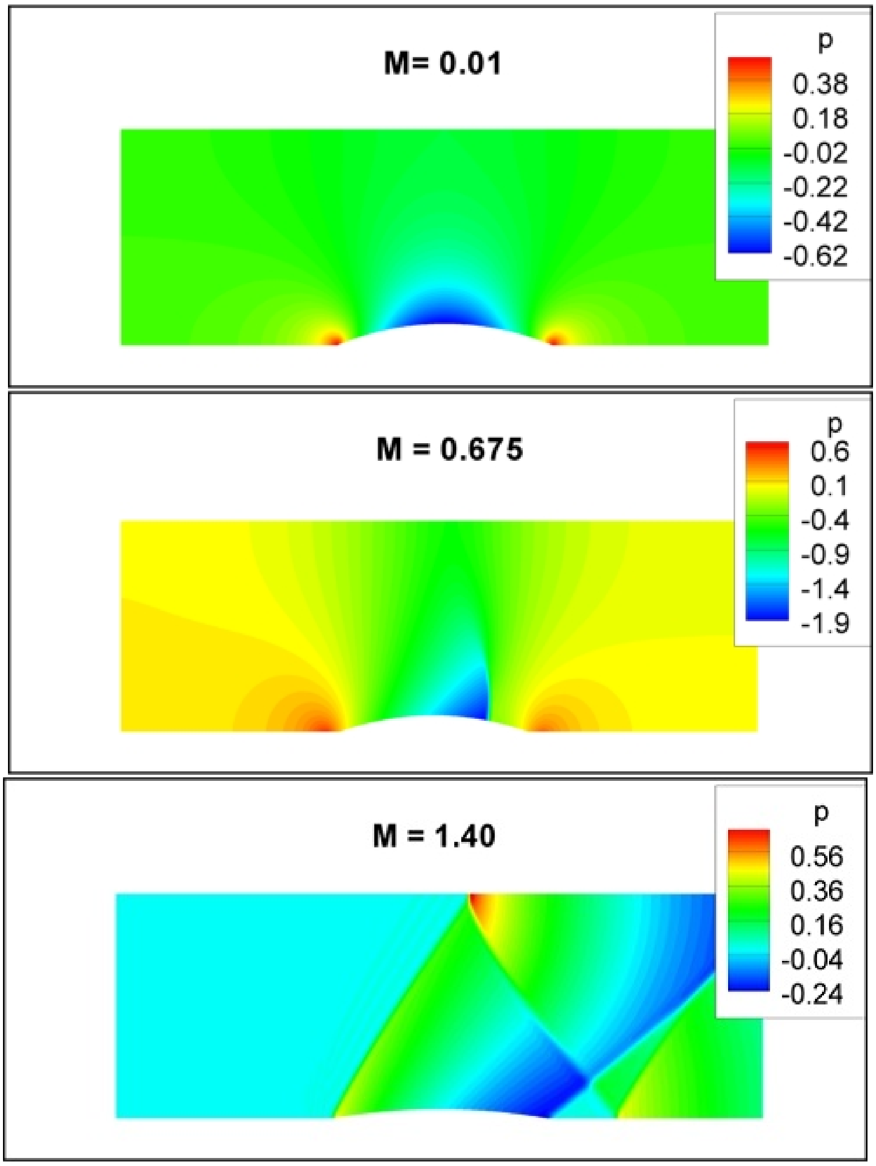

Figure 3.2: Pressure coefficient distributions for channel flows with circular bumps

The Mach number variations on the channel walls are extracted from the converged flow field solutions and used for validation purpose. The resulting distributions are given in Figure 3.3, Figure 3.4 and Figure 3.5. It is observed that the present predictions compare well against the reference study [70].

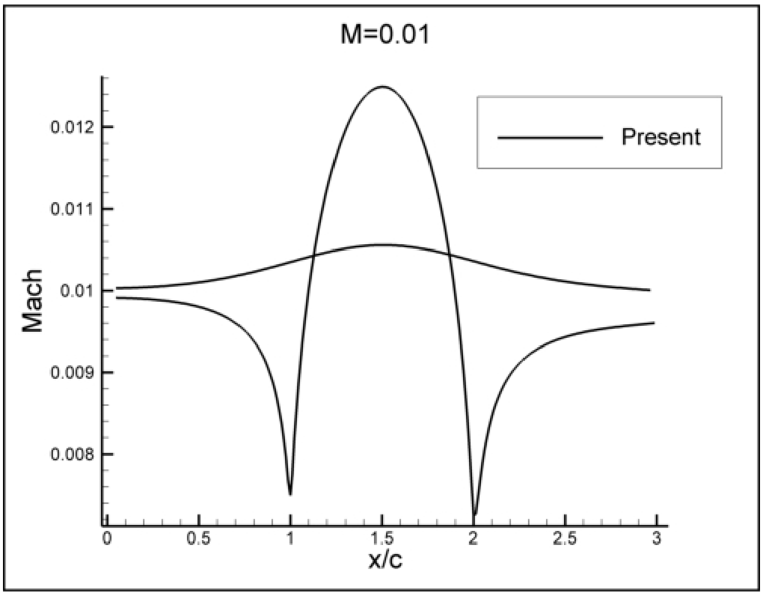

Figure 3.3: Mach number distributions on upper and lower channel walls for $M_\infty = 0.01$

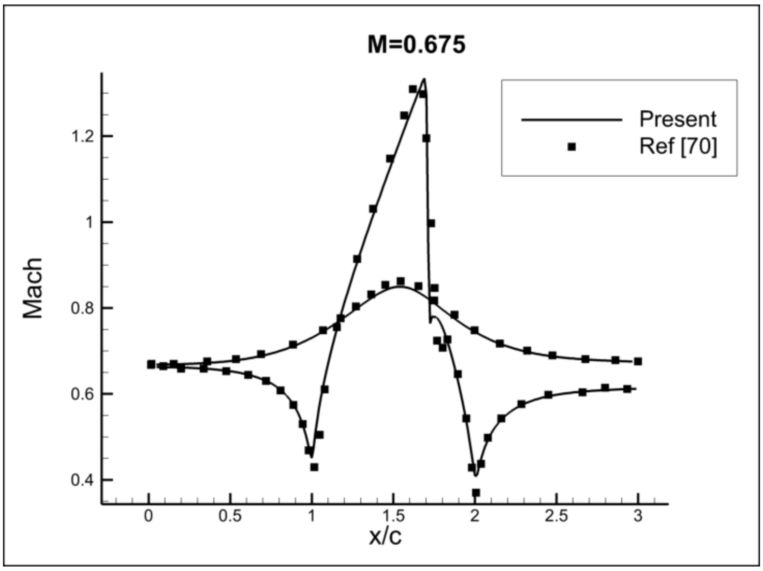

Figure 3.4: Mach number distributions on upper and lower channel walls for $M_\infty = 0.675$

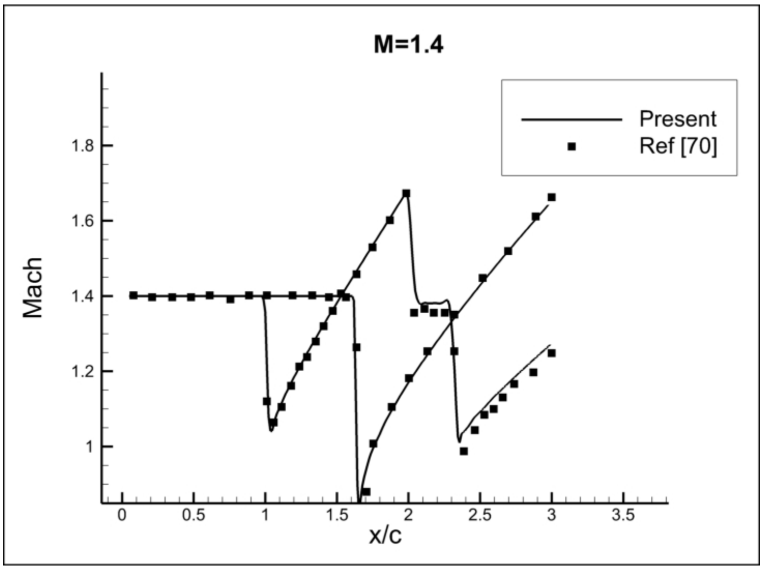

Figure 3.5: Mach number distributions on upper and lower channel walls for $M_\infty = 1.4$

The convergence histories of the present method and the unpreconditioned compressible flow solutions are compared in Figure 3.6 and Figure 3.7 in terms of average residual of flow variables. The compressible solution does not converge for the low Mach number case, whereas the developed method achieves a linear convergence rate. On the other hand, for the transonic case, the convergence rate of the present solution initially behaves similar to that of the compressible solver, but later get worse slightly. Such a deterioration is attributed to the reflective inflow/outflow boundary conditions.

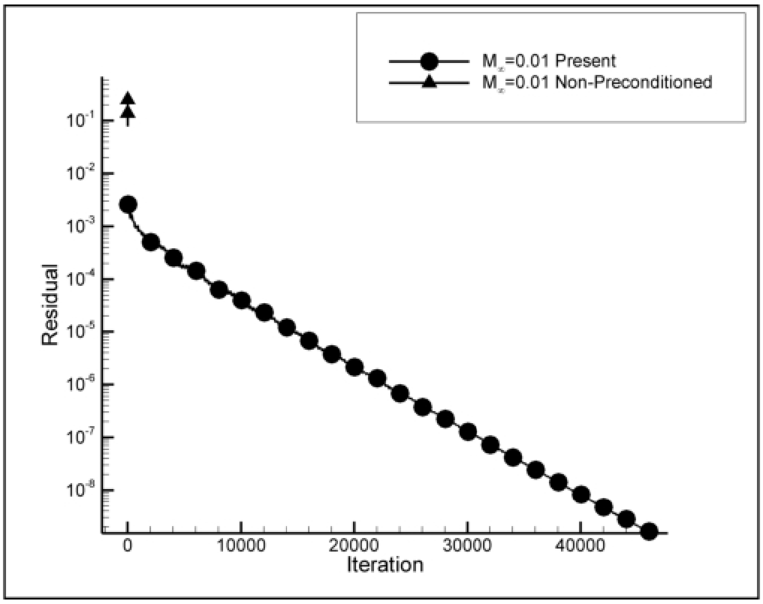

Figure 3.6: Residual histories for subsonic channel flow

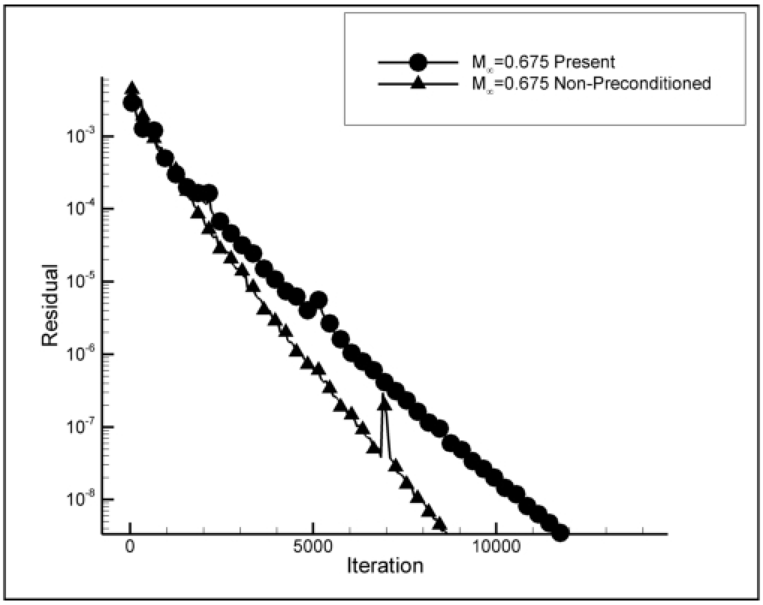

Figure 3.7: Residual histories for transonic channel flow

3.1.1.2 Inviscid Flow over NACA0012 Airfoil

The NACA0012 case starts with a grid independency study and continue with the detailed validation and comparison studies. The grid independency test is conducted for a wide range of Mach numbers $0.0 \leq M_\infty \leq 0.6$ using 3 different

C-type grids for which the grid resolution is quadrupled progressively. The results presented in Table 3.1 show the drag coefficient reduction for all Mach numbers as the grid resolution increases where the correct value is zero for the inviscid solutions.

Table 3.1: Grid Dependency Study for Drag Convergence

	Drag Coefficient							
Grid \ Mach number	0.0	0.1	0.2	0.3	0.4	0.5	0.6	0.7
180x30	0.00148	0.00148	0.00148	0.00149	0.00149	0.00149	0.00148	0.00143
360x60	0.00091	0.00091	0.00091	0.00091	0.00090	0.00089	0.00087	0.00084
720x120	0.00080	0.00080	0.00080	0.00080	0.00079	0.00078	0.00076	0.00073

The 360x60 grid is selected from the grid dependency study and used on the rest of the inviscid 2-D airfoil solutions. The selected computational grid is shown in Figure 3.8.

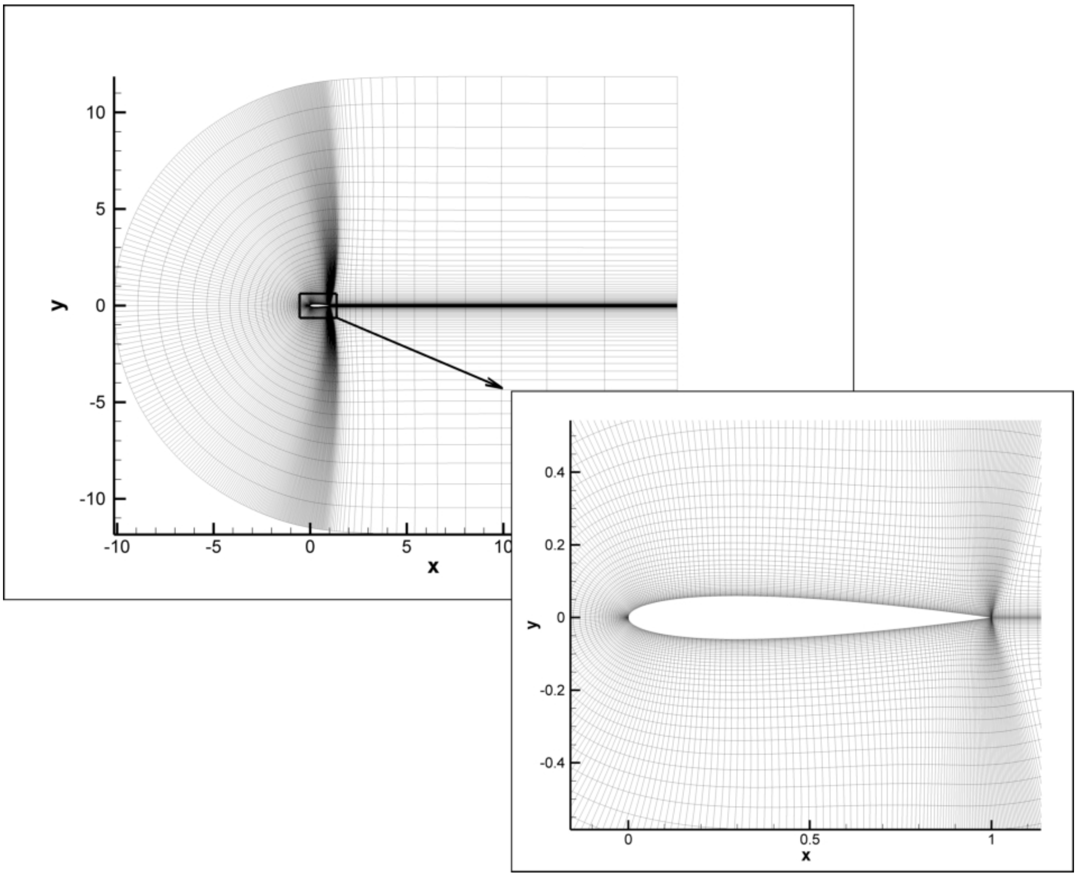

Figure 3.8: The 360x60 C-type grid around NACA 0012 airfoil

The convergence rate of the present preconditioner is next compared against two other similar studies, one of which is based on Rossow's formulation [50], and the other one is based on Turkel's formulation [71]. In these comparison cases, the inviscid flows over NACA 0012 airfoil are computed using Roe upwinding and Runge Kutta time stepping with similar mesh sizes. The study on [50] and [71] employ first and second order spatial discretizations respectively. The same discretization order is used with the present formulation for each case. Reference [50] also employs 10 sub-iterations in each Runge-Kutta stage which is not implemented in the current study. As observed in Figure 3.9 and in Figure 3.10, the present solution has a comparable convergence rate with that of [50] in spite of the sub-iterations employed on the latter. On the other hand, the present method has a significantly better convergence rate than [71].

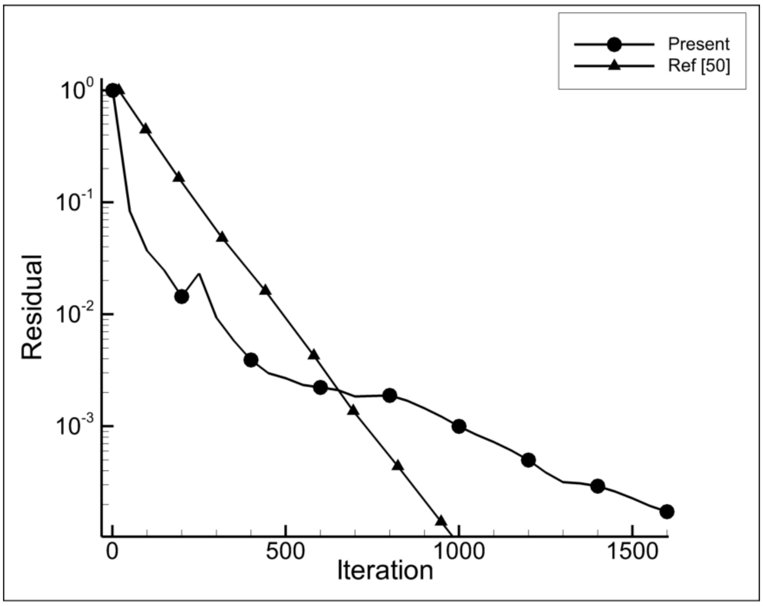

Figure 3.9: Comparison of convergence rate with Reference [50]

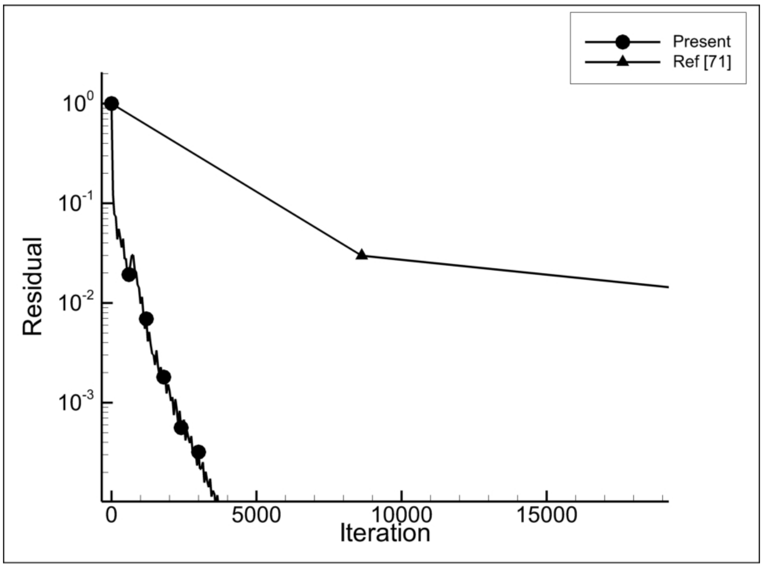

Figure 3.10: Comparison of convergence rate with Reference [71]

Although the present results show a comparable performance, it should be noted that there are various factors which effect the convergence character of the solutions. For a quantitative comparison, non-preconditioned formulations should have the same discretization schemes, boundary conditions and solution algorithms.

As the validation study for spatial accuracy, the incompressible and a low Mach number of $M_\infty = 0.001$ flow solutions are obtained on the 360x60 grid. These solutions are compared with the incompressible flow solutions obtained by the ACM formulation and by a panel method in Figure 3.11. As shown, the present method predicts the surface pressure coefficient distribution accurately. Furthermore, the residual histories given in Figure 3.12 show that the convergence rate of the present preconditioner for $M_\infty = 0.01$ and $M_\infty = 0$ are almost identical with each other and about the same as the ACM method.

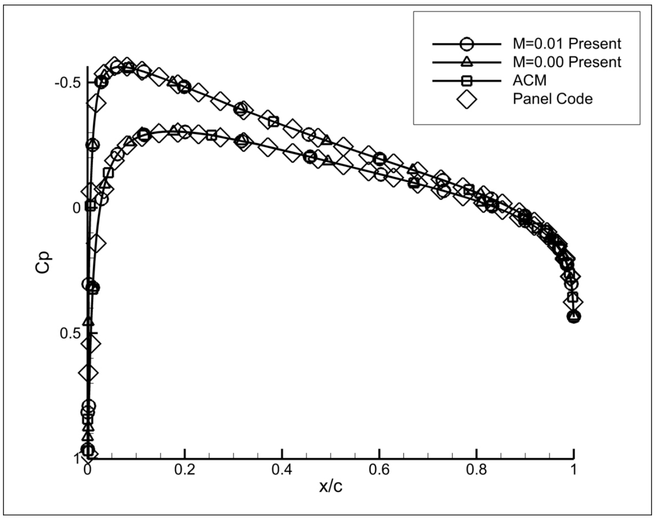

Figure 3.11: Surface pressure coefficient distributions for incompressible flows over NACA0012 airfoil

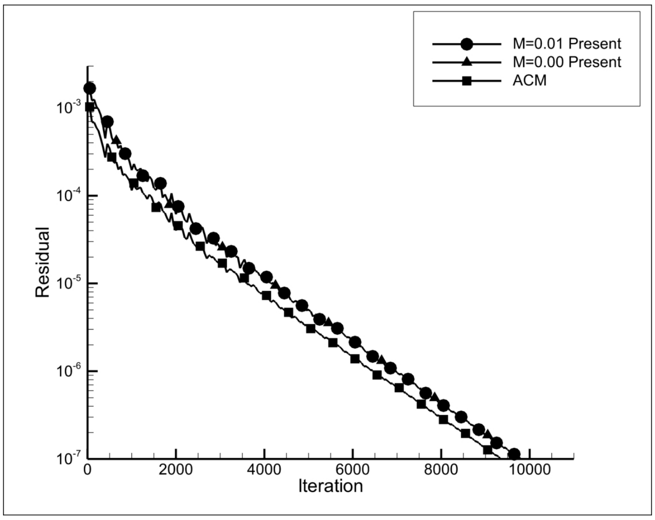

Figure 3.12: Residual histories for incompressible flows over NACA0012 airfoil

The preconditioned solution at $M_\infty = 0.01$ is next compared against the non-preconditioned solution in Figure 3.13 and Figure 3.14. Although the pressure coefficient distributions, in general, agree well, the non-preconditioned flow solution exhibits the expected slow convergence and regional stability issues. The stability of the non-preconditioned solution deteriorates especially at the stagnation region due to numerical pressure oscillations.

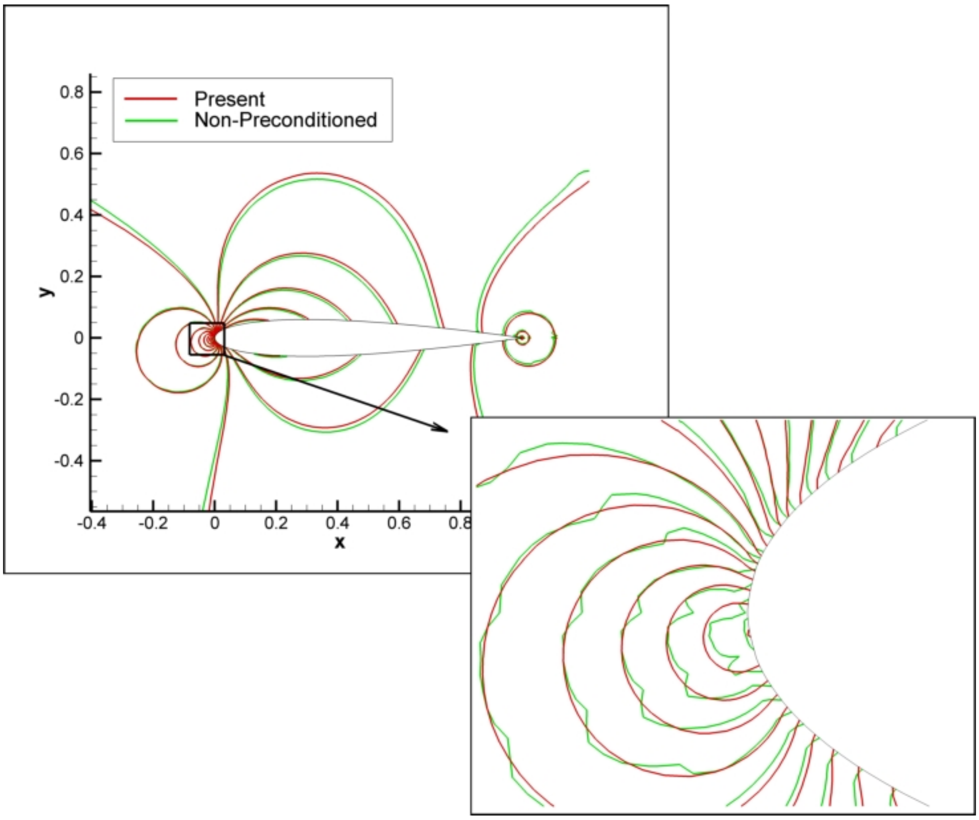

Figure 3.13: Pressure coefficient distributions for flow over NACA0012 airfoil at $M_\infty = 0.01$

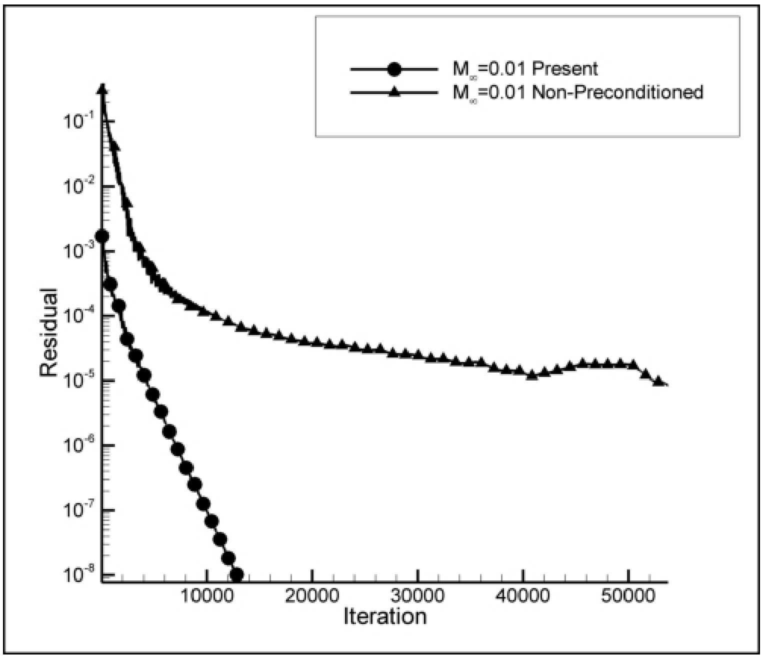

Figure 3.14: Residual histories for flow over NACA0012 airfoil at $M_\infty = 0.01$

The accuracy and performance of the present preconditioner are also evaluated at high subsonic and transonic flow conditions. The flow solutions with and without the preconditioner are first presented for $M_\infty = 0.50$. The Mach number distributions and the residual histories are compared in Figure 3.15 and Figure 3.16. As shown, the accuracy and the convergence acceleration of the preconditioned solutions at the selected high subsonic Mach number solution are consistent with each other.

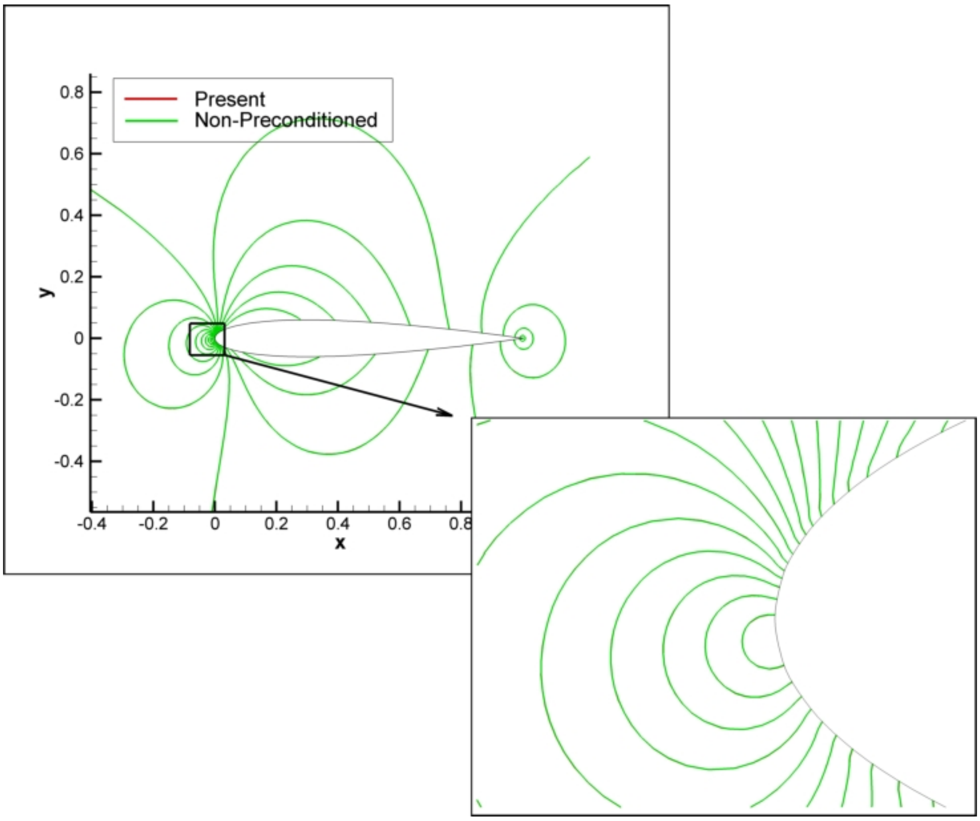

Figure 3.15: Pressure coefficient distributions for flow over NACA0012 airfoil at $M_\infty = 0.5$

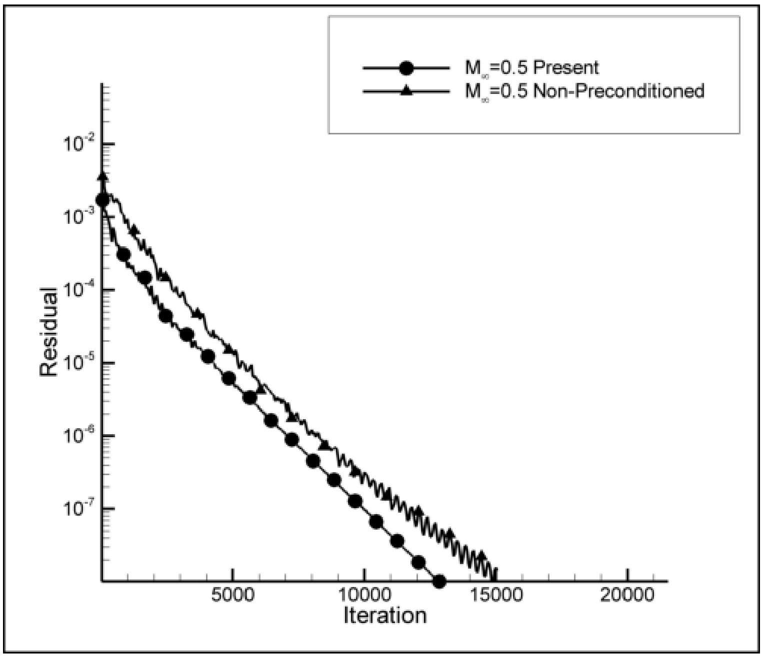

Figure 3.16: Residual histories for flow over NACA0012 airfoil at $M_\infty = 0.5$

Next, the transonic flow at $M_\infty = 0.855$, which is a widely used AGARD [72] test case for compressible flow solvers, is considered. As shown in Figure 3.17, Figure 3.18 and Figure 3.19, the predictions of the shock locations with and without the preconditioner are about the same, and both agree well with the AGARD data. In addition, the convergence rate of the preconditioned solution still does not deteriorate at transonic flow conditions.

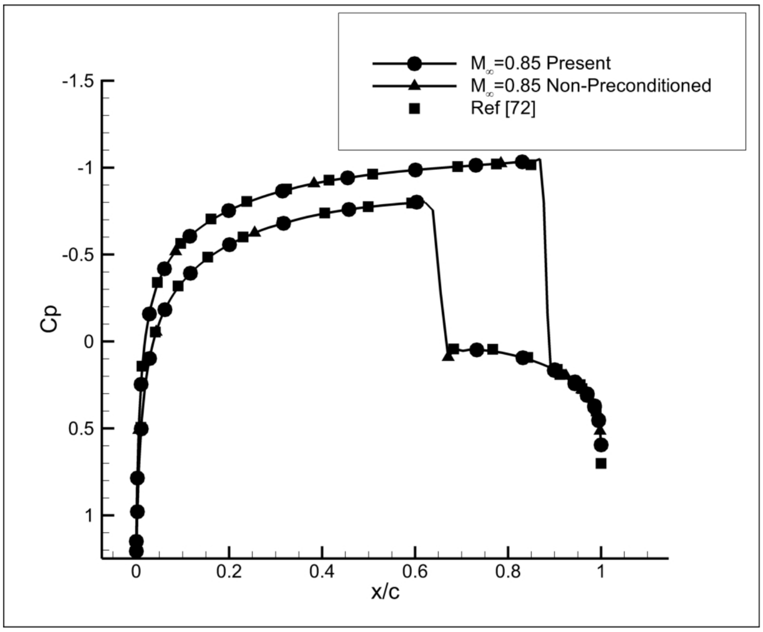

Figure 3.17: Surface pressure coefficient distribution for flow over NACA0012 airfoil at $M_\infty = 0.855$

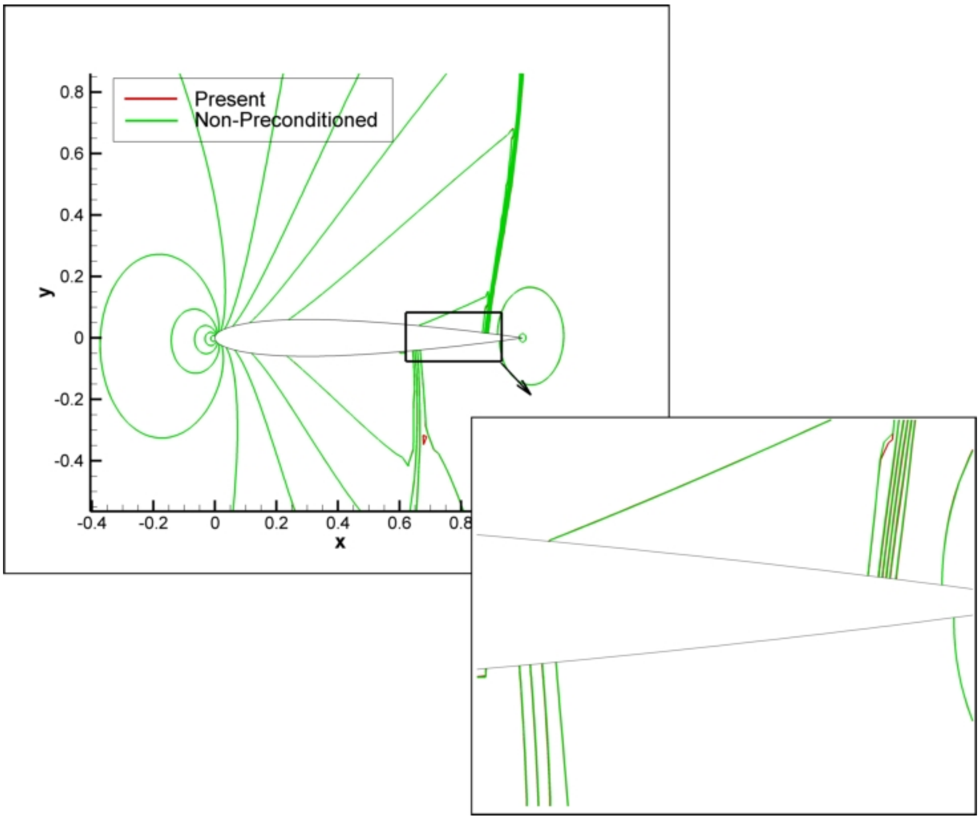

Figure 3.18: Pressure coefficient distributions for flow over NACA0012 airfoil at $M_\infty = 0.855$

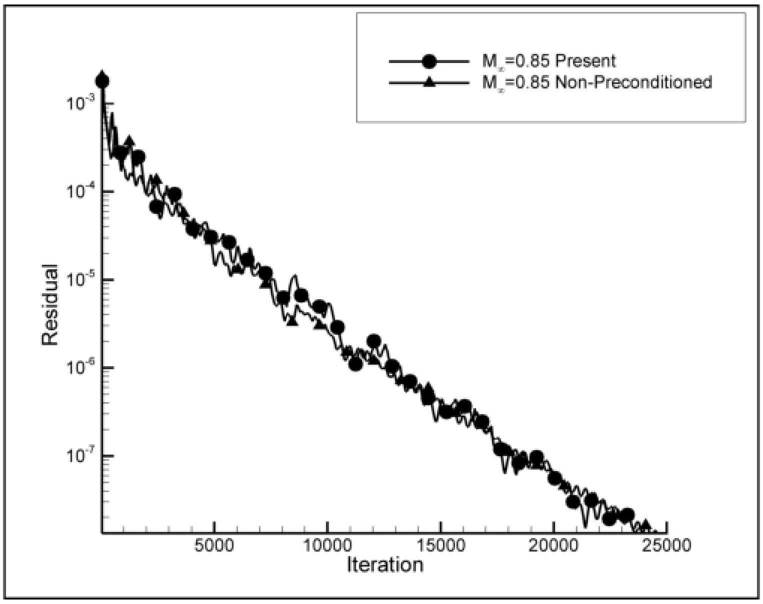

Figure 3.19: Residual histories for flow over NACA0012 airfoil at $M_\infty = 0.855$

The convergence characteristics of the present preconditioner are presented for the whole subsonic Mach numbers range in Figure 3.20. It is observed that almost a uniform convergence rate is achieved for all Mach number flows up to $M_\infty = 0.5$ including $M_\infty = 0$ case, which shows the Mach uniform solution efficiency of the present preconditioner.

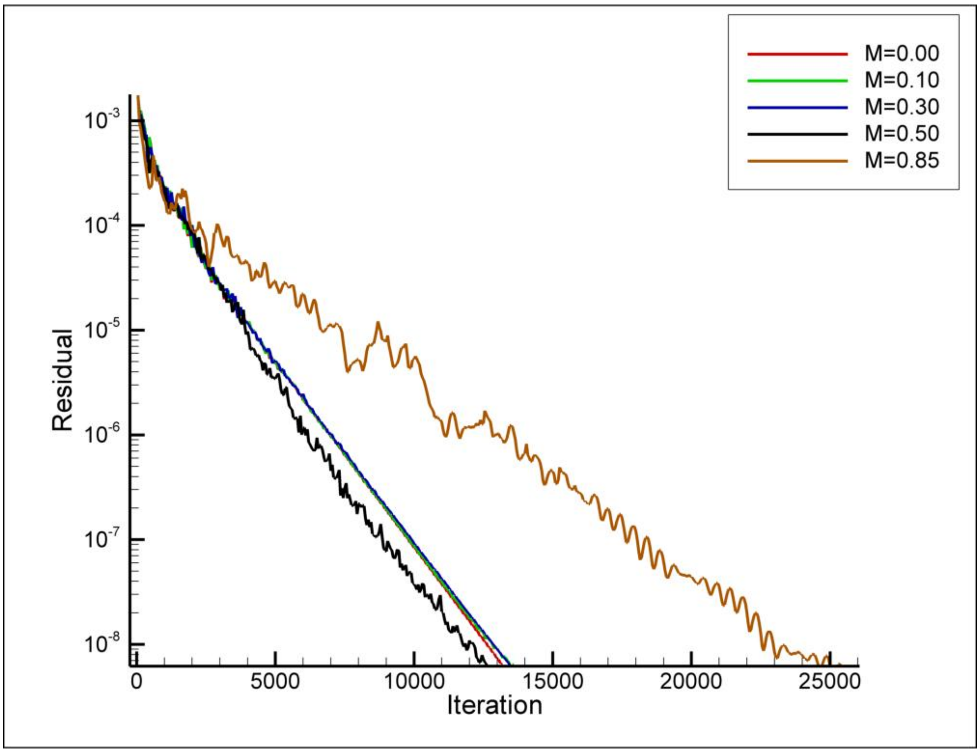

Figure 3.20: Residual histories for flows over NACA0012 airfoil

3.1.2 Viscous Flow Cases

The preconditioned governing equations given in Equation 2.20 contains the viscous terms and how they are treated in the present preconditioning formulation. The viscous residual terms of conservation of momentum equations are also added to the conservation of energy equation in their discretized forms within preconditioning method. Since the viscous fluxes are in elliptical character, the addition of their residuals does not effect the eigenstructure of the governing equations.

The cases studied for viscous flows are conducted to demonstrate that the present preconditioning formulation does not exhibit any stability problem due to the diffusive terms of the Navier-Stokes equations. In this context, viscous flows over a flat plate and NACA0008 airfoil are studied.

3.1.2.1 Viscous flow over a flat plate

As a standard test case, viscous flow over a flat plate with zero pressure gradient is firstly analyzed to validate the proposed Navier-Stokes preconditioning formulation. The well known Blasius solution is used as the validation data of skin friction coefficient distribution for the incompressible flow. A cartesian 190x70 algebraic grid is generated where the grid points are clustered near leading edge and boundary layer. The grid is shown in Figure 3.21.

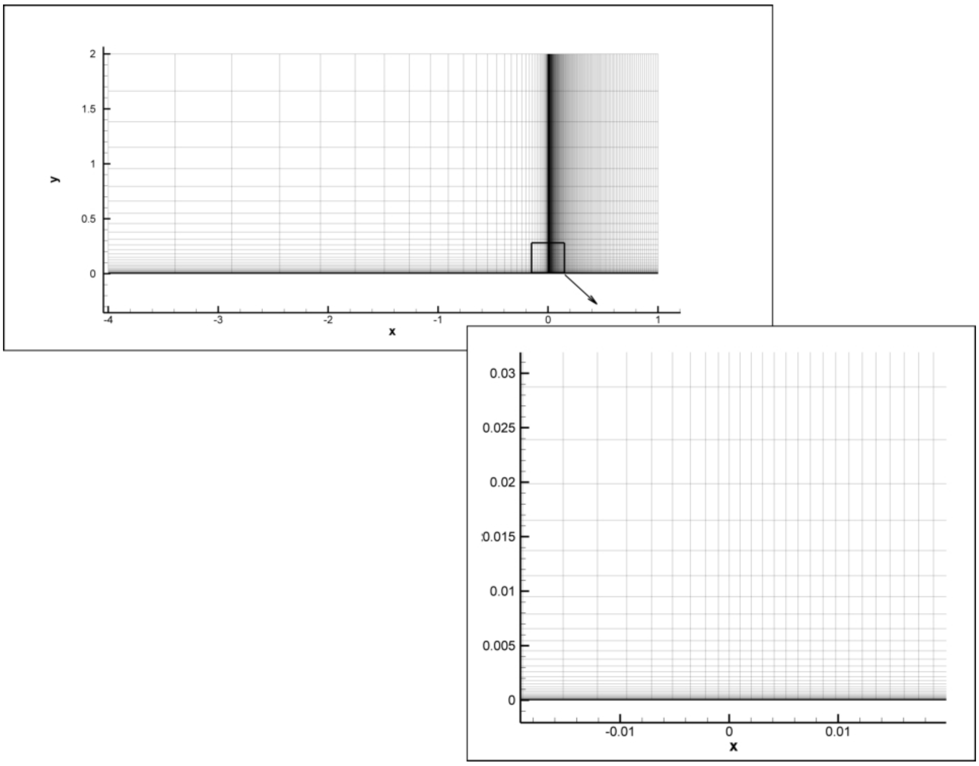

Figure 3.21: Computational grid over flat plate

The variation of local skin friction coefficient with the local Reynolds number is compared with the Blasius solution which is calculated with the formula:

$$c_f = \frac{0.664}{\sqrt{Re_x}}$$

where $Re_x = \frac{\rho U x}{\mu}$ is the local Reynolds number.

The comparison of skin friction coefficient distribution is shown in Figure 3.22

where a good agreement is obtained.

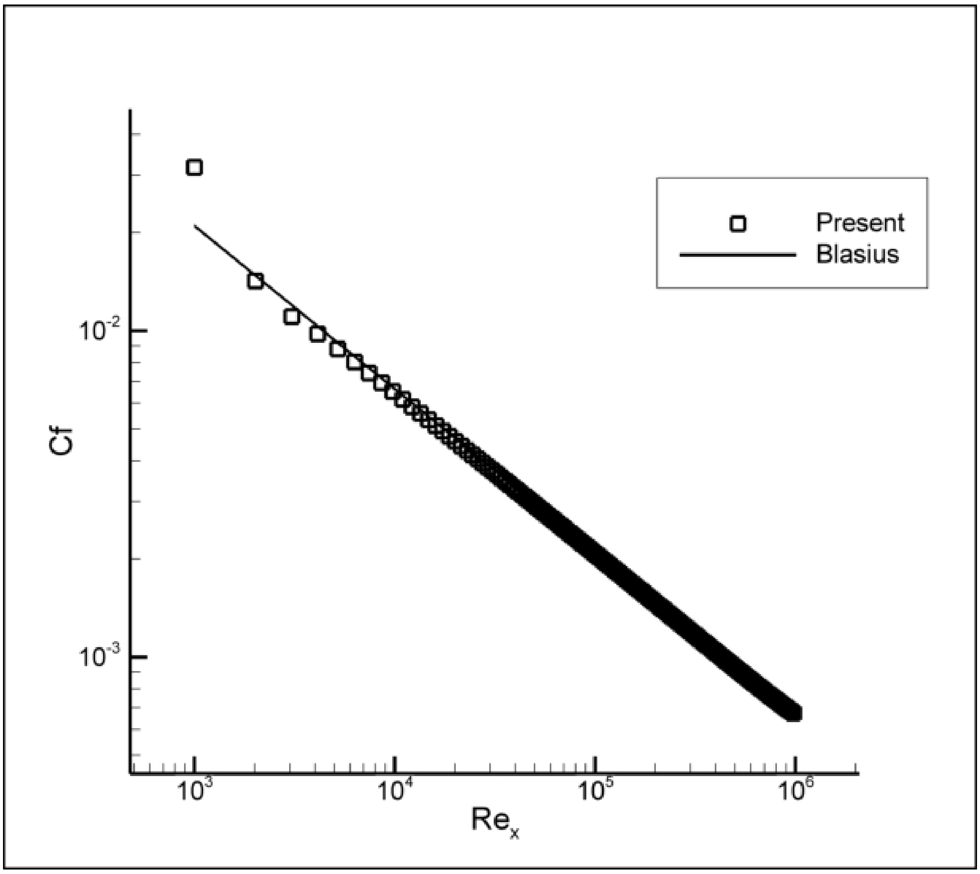

Figure 3.22: Comparison of the computed skin friction coefficient with the Blasius solution

3.1.2.2 Viscous Flow over a NACA0008 Airfoil

Low Reynolds number flows over a NACA0008 airfoil are selected as the second set of validation cases for implementation of the viscous terms. 2-D structured 260x40 grid is again generated with the in-house hyperbolic grid generator [59] and shown in Figure 3.23.

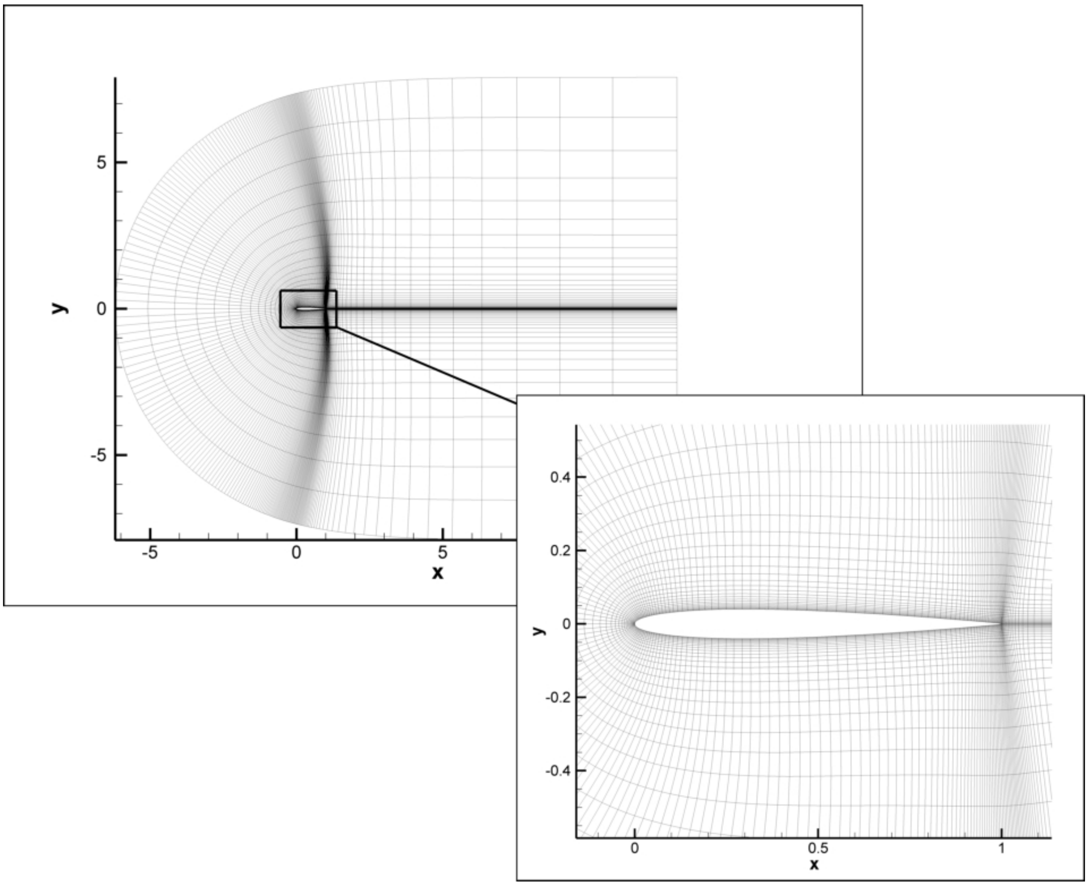

Figure 3.23: The 260x40 C-type grid around NACA 0008 airfoil

As the first laminar case for NACA0008 airfoil, zero angle of attack incompressible flow with 2000 and 6000 Reynolds numbers are solved and the pressure coefficient distributions are compared with [73]. The obtained results, shown in Figure 3.24, are consistent with the solutions given in [73].

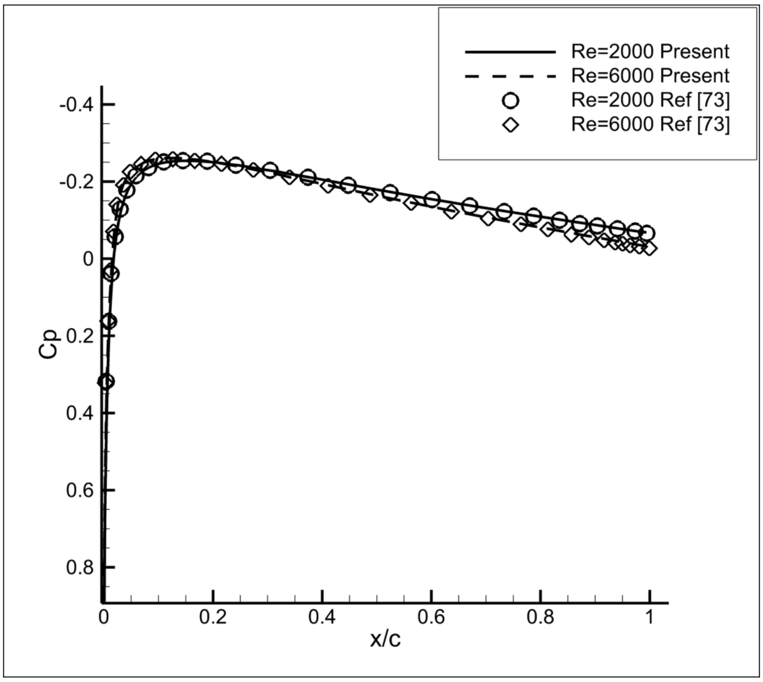

Figure 3.24: Surface pressure coefficient distribution for flow over NACA0008 airfoil at $M_\infty = 0.0$ and $\alpha = 0°$

$Re = 6000$ flow with $\alpha = 2°$ is also solved and the resulting pressure coefficient distribution are compared with [73].

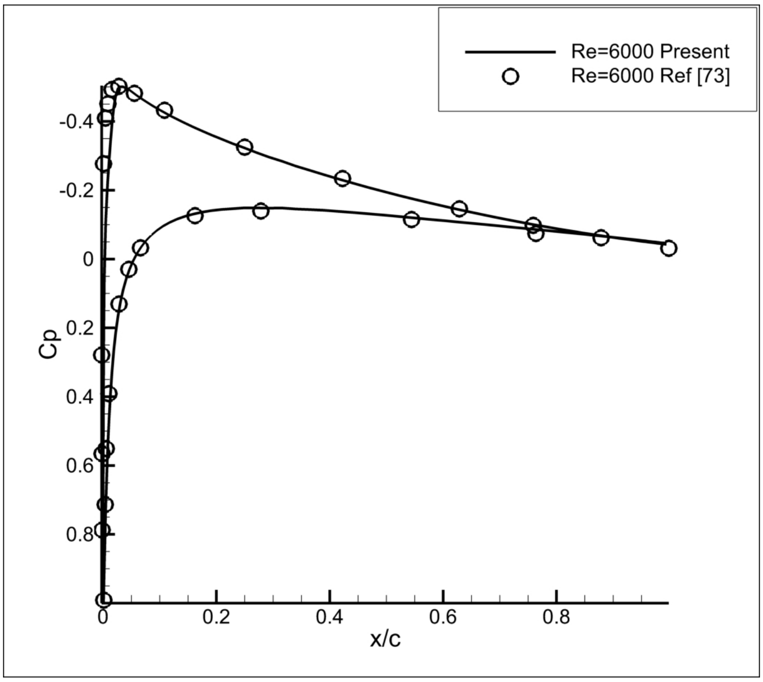

Figure 3.25: Surface pressure coefficient distribution for flow over NACA0008 airfoil at $M_\infty = 0.0$, $Re = 6000$ and $\alpha = 2°$

The $\alpha = 2°$ and $Re = 6000$ flow case is approximately the condition where the trailing edge seperation starts. Streamlines on the trailing edge of NACA0008 airfoil for $\alpha = 2°$, $\alpha = 3°$ and $\alpha = 4°$ are visualized in Figure 3.26.

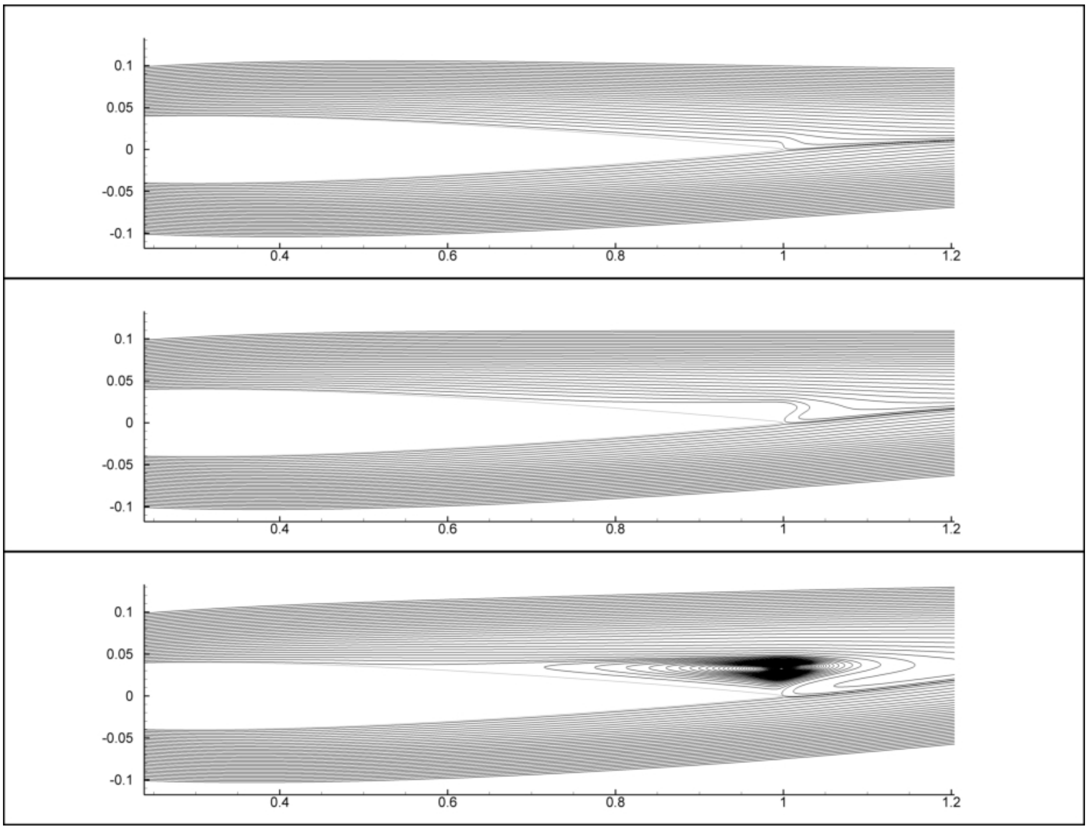

Figure 3.26: Streamlines on the trailing edge of NACA0008 airfoil on different angle of attack values

As the last 2-D laminar flow test cases, preconditioned and non-preconditioned solutions for $M_\infty = 0.01$ and $M_\infty = 0.5$ are solved. The resulting velocity magnitude contours and velocity vectors are compared in Figure 3.27 and in Figure 3.28. It is observed that the difference between the preconditioned and non-preconditioned solutions are negligible for $M_\infty = 0.5$ whereas non-preconditioned solution considerably inaccurate on $M_\infty = 0.01$ flow case as expected.

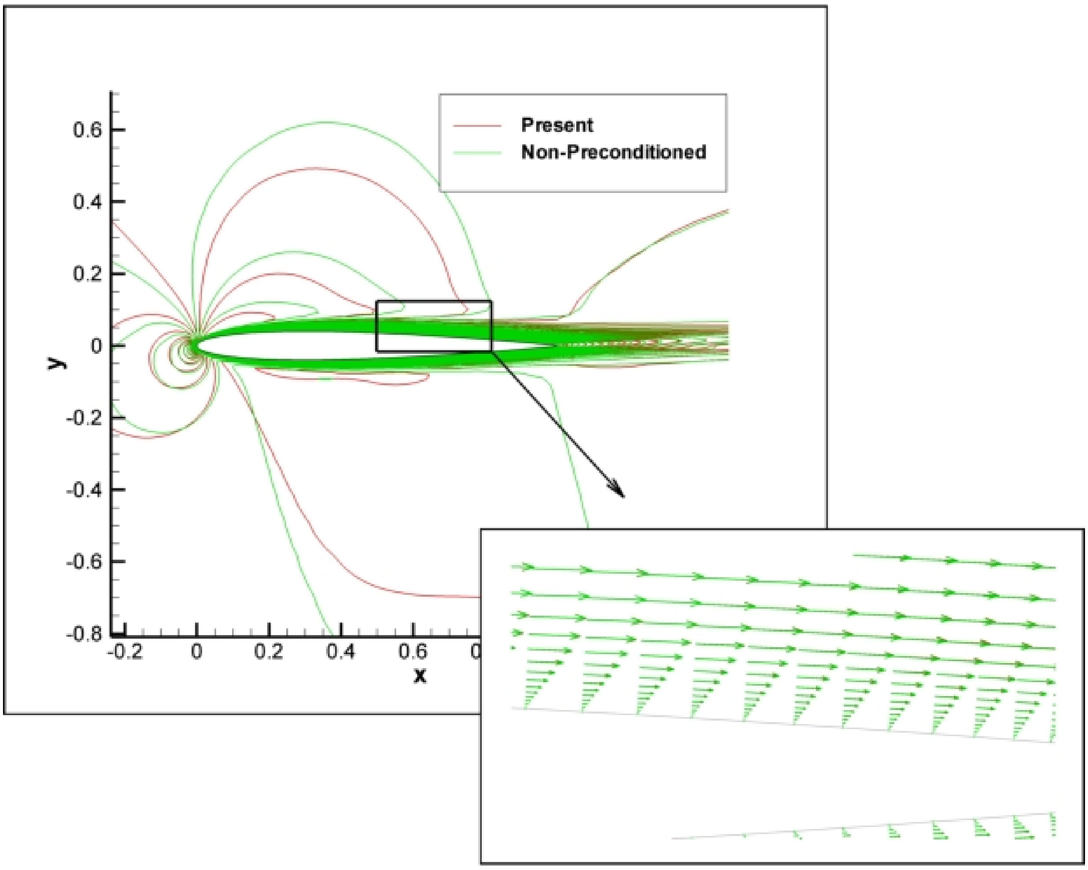

Figure 3.27: Velocity magnitude distribution of preconditioned and non-preconditioned flow solutions over NACA0008 airfoil at $M_\infty = 0.01$, $Re = 6000$ $\alpha = 2°$

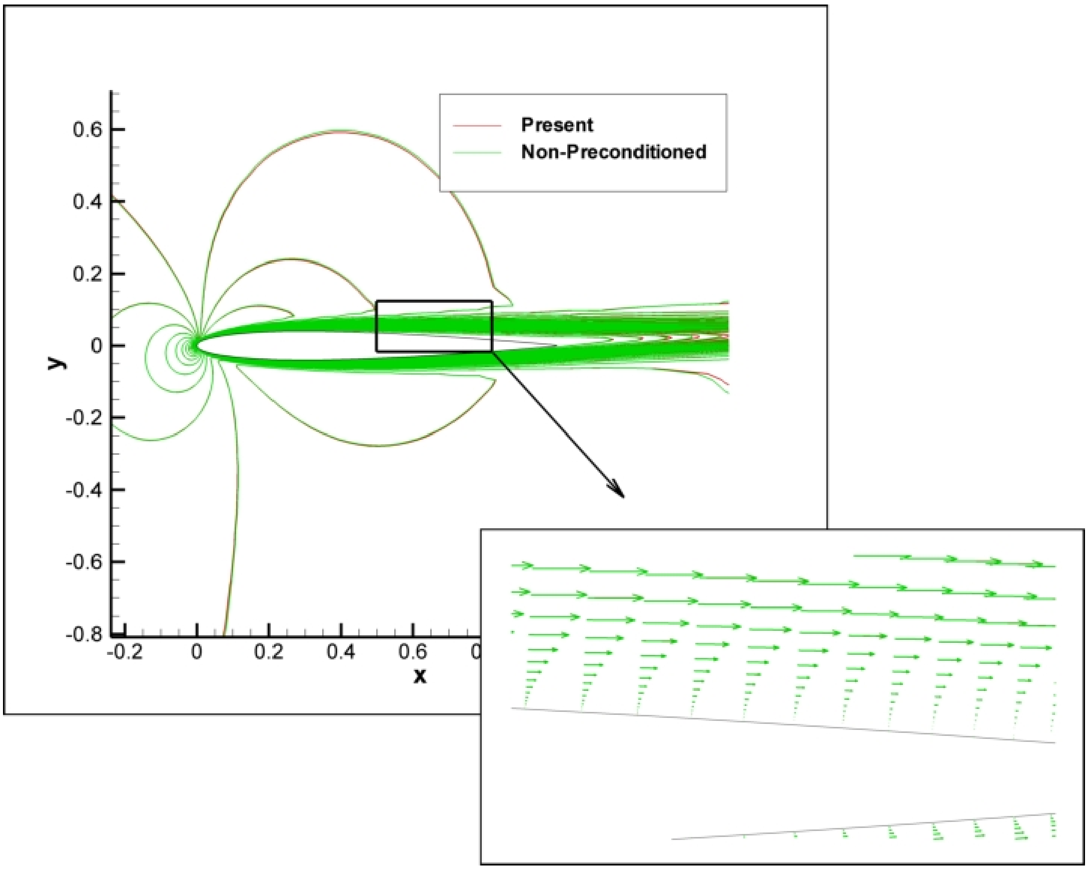

Figure 3.28: Velocity magnitude distribution of preconditioned and non-preconditioned flow solutions over NACA0008 airfoil at $M_\infty = 0.5$, $Re = 6000$ $\alpha = 2°$

3.2 Three Dimensional Cases

Two different 3-D test case sets are selected both for validation and performance evaluation purposes. These test cases are the inviscid flows over ONERA M6 wing and the viscous flows over DLR-F4 wing body geometry.

3.2.1 Inviscid Flow over ONERA M6 Wing

ONERA M6 wing has a relatively simple geometry with no twist and a symmetrical airfoil. This test case is mainly selected because of its wide usage as a standard test case for the developed CFD codes. Among various free stream Mach numbers and angle of attacks, Test 2308 of [74] is selected where $M_\infty = 0.8395$ and $\alpha = 3.06$. A 3-D unstructured mesh with 447842 tetrahedral cells and 91418 nodes is generated and used. This grid is shown in Figure 3.29.

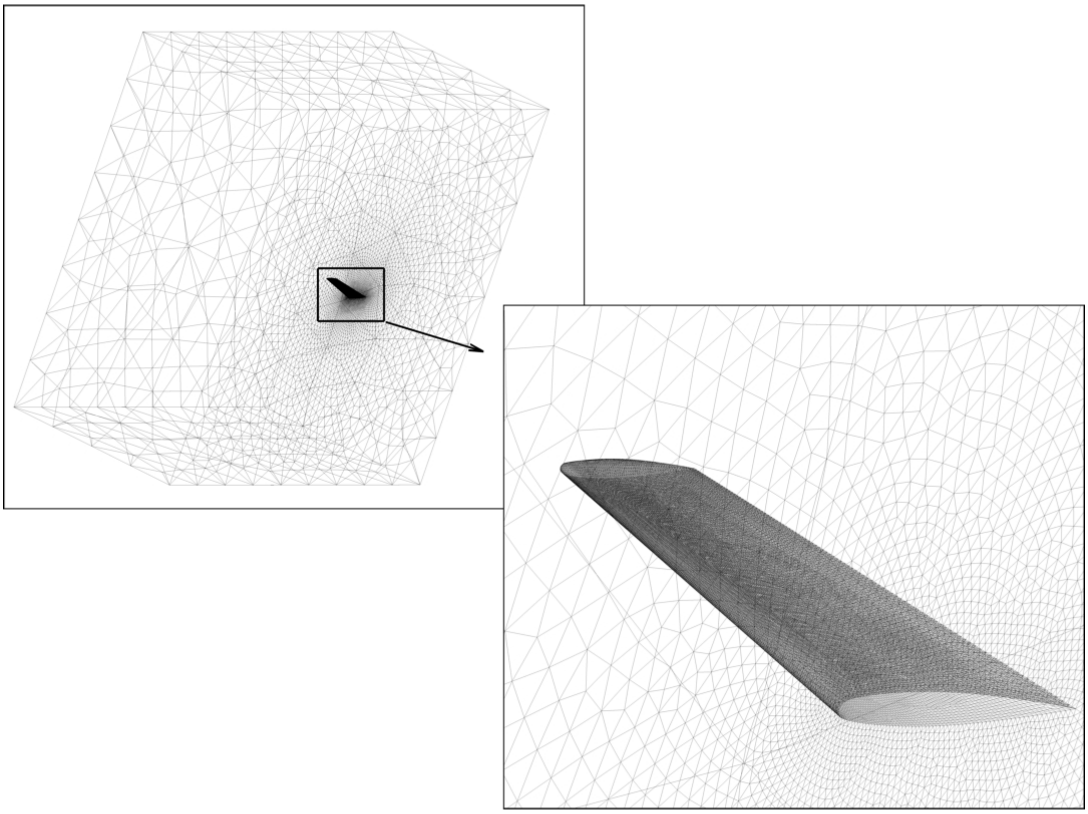

Figure 3.29: Computational grid employed for ONERA M6 wing

In Figure 3.30 and Figure 3.31, the distribution of pressure coefficient over two different spanwise locations are compared against the experimental data. As expected, the preconditioned and non-preconditioned solutions are the same at both stations and the inviscid flow prediction is in better agreement with the experimental data at station $y/b = 0.2$. The disagreement at station $y/b = 0.95$ is attributed to the viscous effects due to tip vortex.

Since first order spatial discretization is employed, a relatively high diffusivity is also observed especially on the suction peak locations.

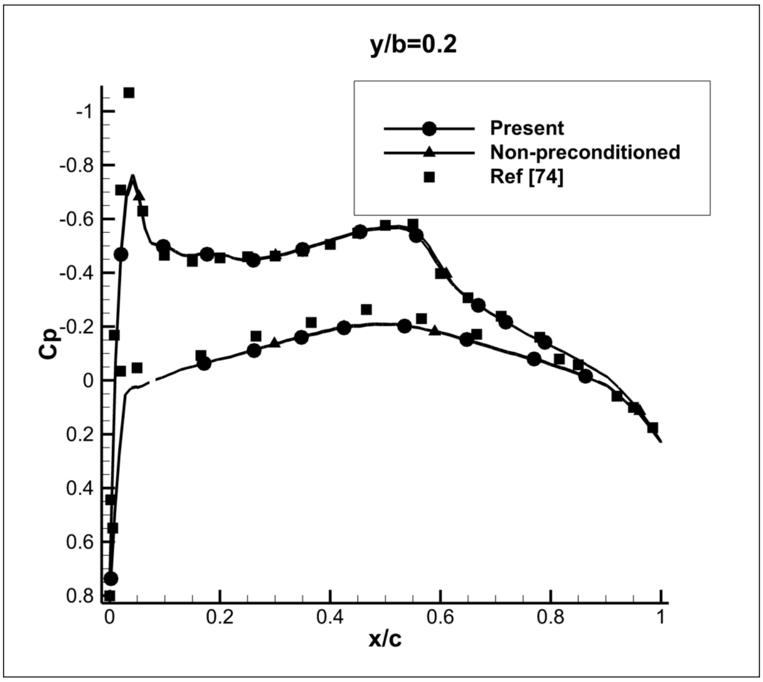

Figure 3.30: Pressure coefficient distributions for flow over ONERA M6 wing at $y/b = 0.2$

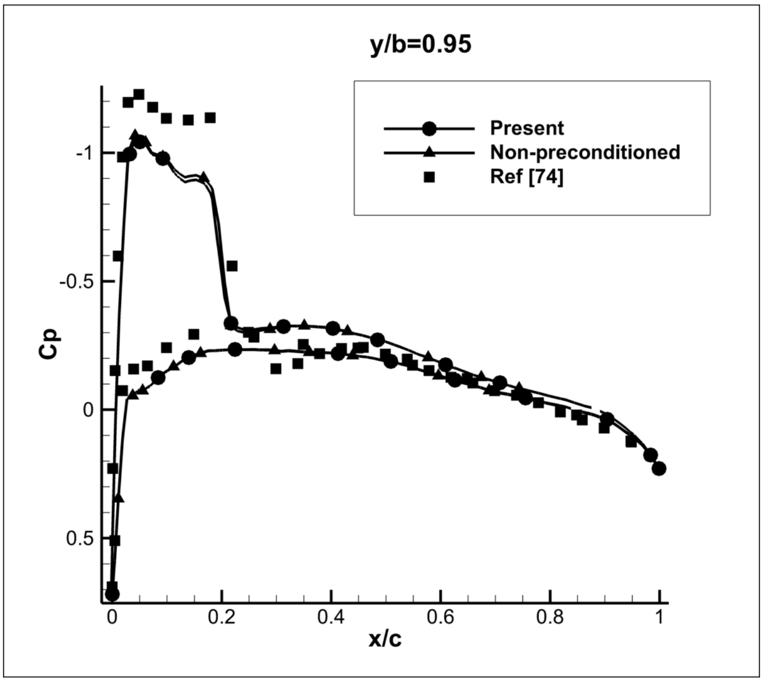

Figure 3.31: Pressure coefficient distributions for flow over ONERA M6 wing at $y/b = 0.95$

After the validation of the developed 3-D formulation, its impact on the convergence characteristics is analyzed on a range of free stream Mach numbers from incompressible to transonic speeds. In all the cases, the CFL value is kept at its highest values while the solution stability is achieved. It is observed that, while maximum CFL values occur to be around 3 for all preconditioned cases, CFL values as low as 0.01 are needed for non-preconditioned solutions.

The pressure coefficient distribution and the residual histories are presented in Figure 3.32 to Figure 3.41 where 0.5m span location is selected for comparison.

The flow condition of $M_\infty = 0.005$ is selected as the first 3-D performance comparison case. The preconditioned and non-preconditioned solutions are given in Figure 3.32 and Figure 3.33 with their convergence histories. The pressure coefficient distributions are in good agreement in general but the non-preconditioned flow solution exhibits the expected slow convergence and regional stability issues as in the case of 2-D solutions.

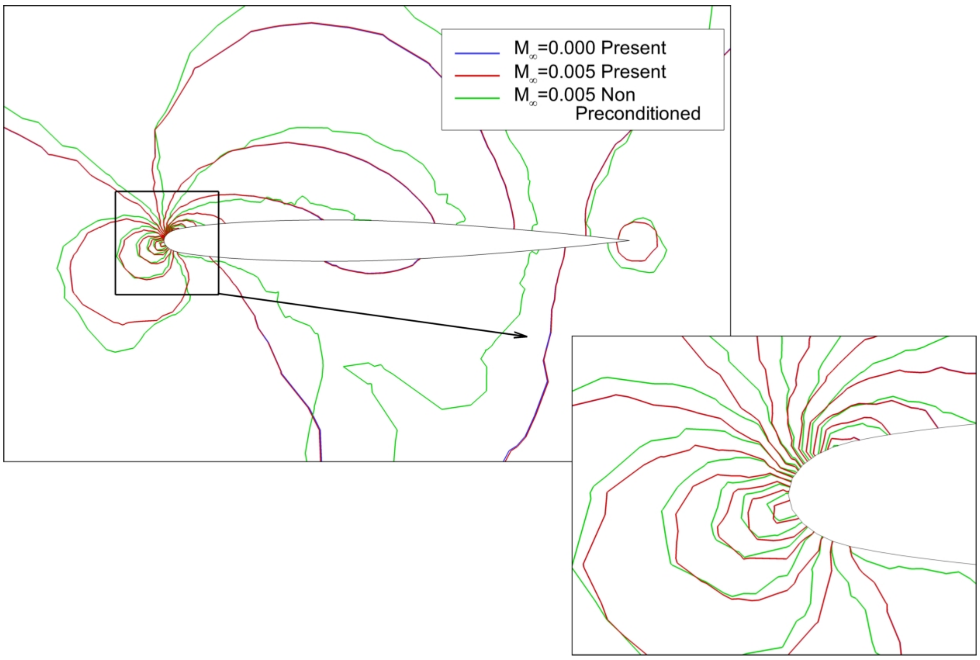

Figure 3.32: Pressure coefficient distributions for flow over ONERA M6 wing at $M_\infty = 0.005$

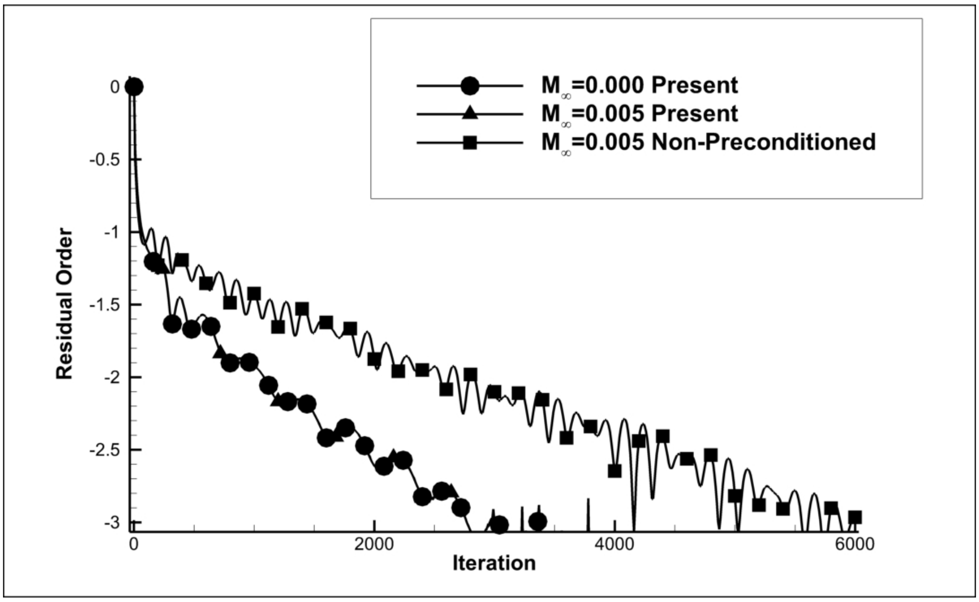

Figure 3.33: Residual histories for flow over ONERA M6 wing at $M_\infty = 0.005$

The accuracy and performance of the present preconditioner are also evaluated at 3-D low and high subsonic flow conditions where a considerable difference is expected neither in solution flow field nor in the residual history. The comparison graphs from Figure 3.34 to Figure 3.39 verify that any deterioration is not observed on $M_\infty = 0.1$, $M_\infty = 0.3$ and $M_\infty = 0.5$ cases.

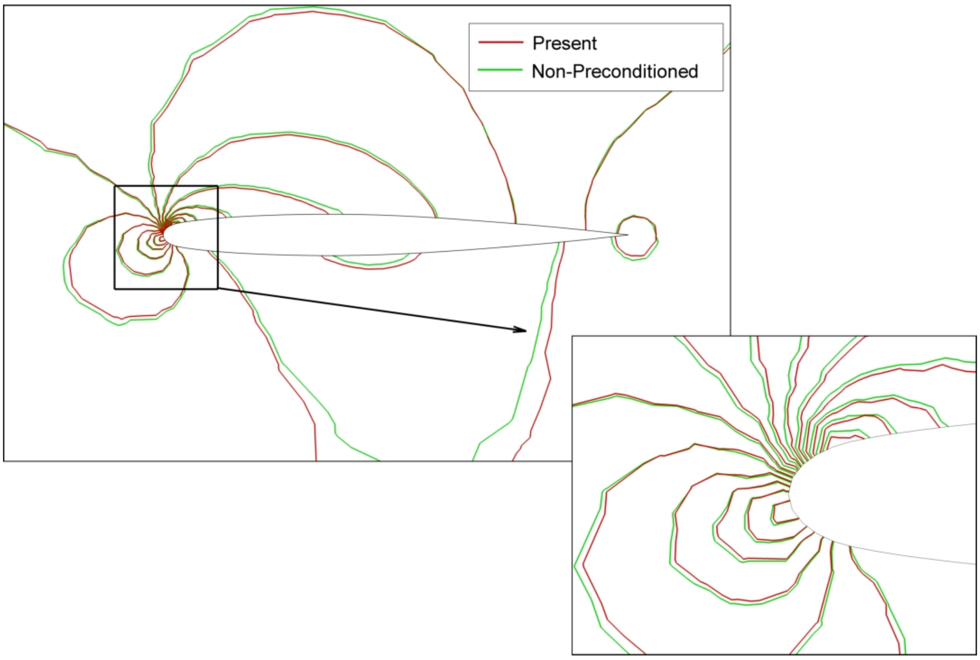

Figure 3.34: Pressure coefficient distributions for flow over ONERA M6 wing at $M_\infty = 0.1$

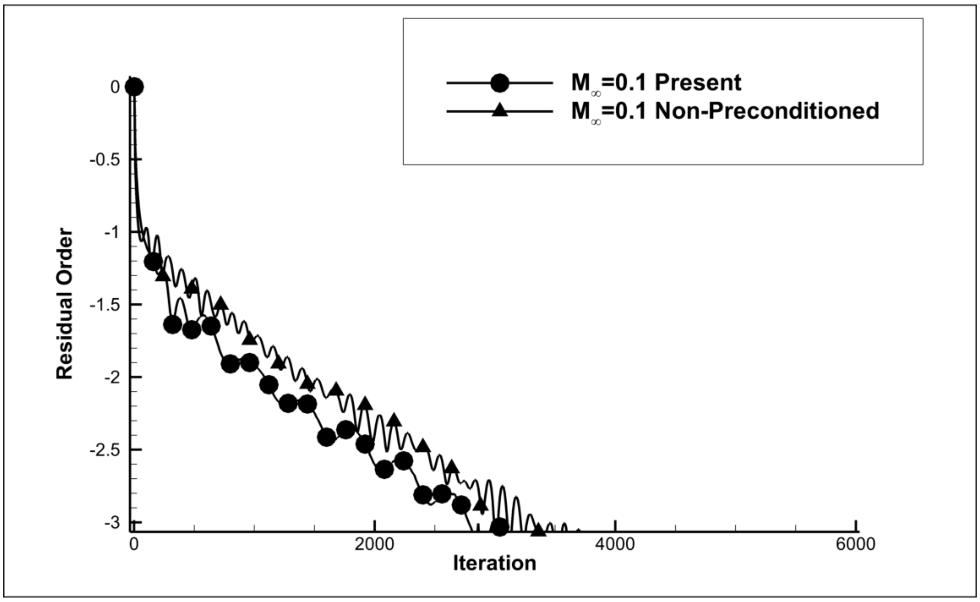

Figure 3.35: Residual histories for flow over ONERA M6 wing at $M_\infty = 0.1$

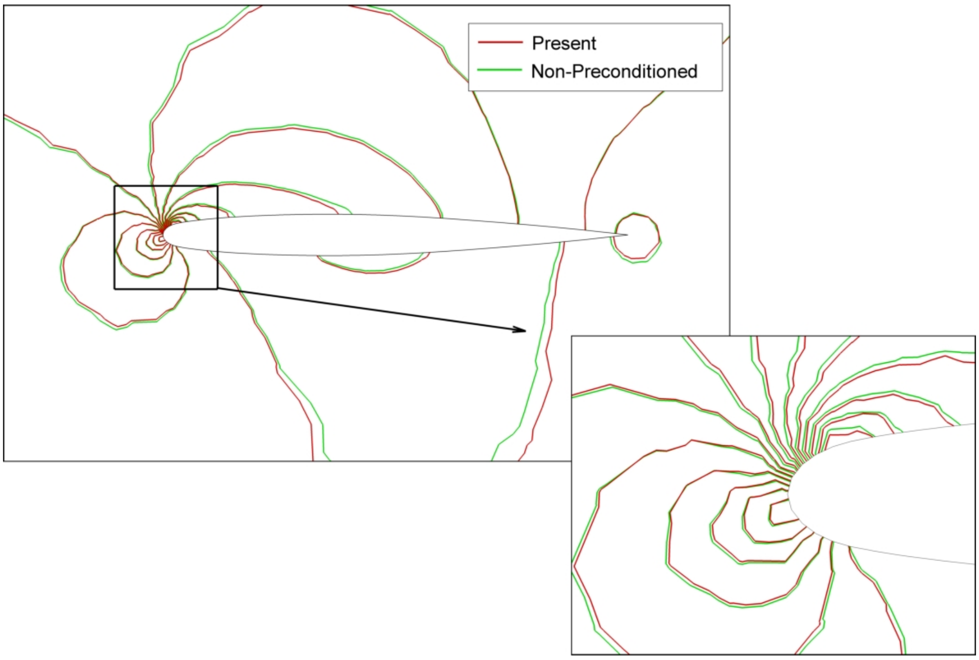

Figure 3.36: Pressure coefficient distributions for flow over ONERA M6 wing at $M_\infty = 0.3$

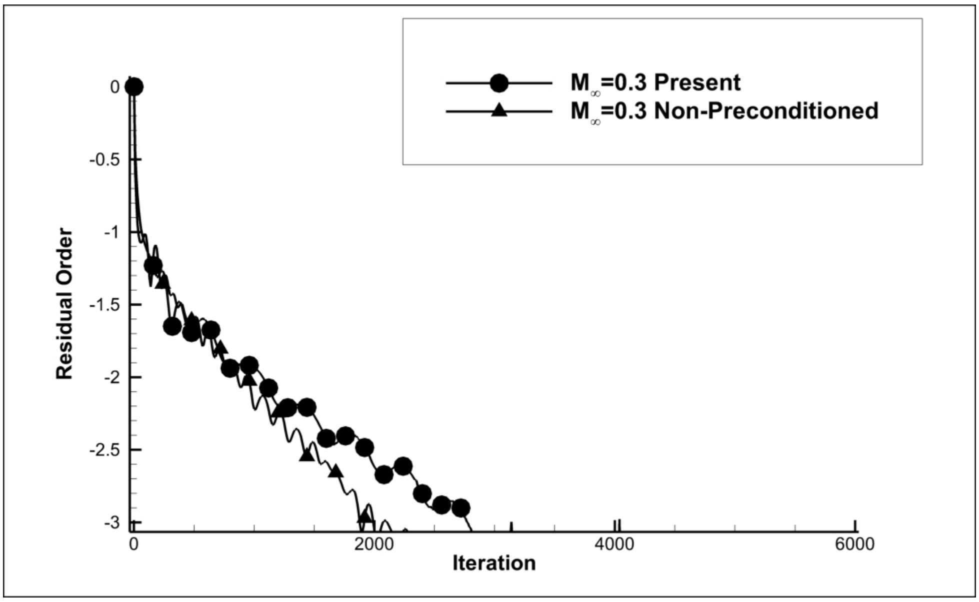

Figure 3.37: Residual histories for flow over ONERA M6 wing at $M_\infty = 0.3$

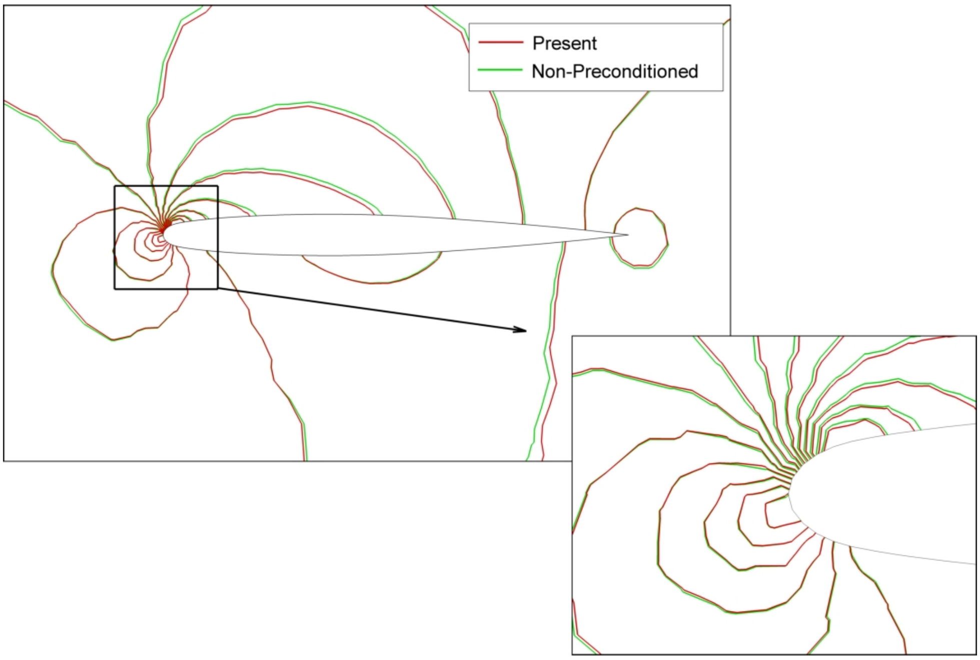

Figure 3.38: Pressure coefficient distributions for flow over ONERA M6 wing at $M_\infty = 0.5$

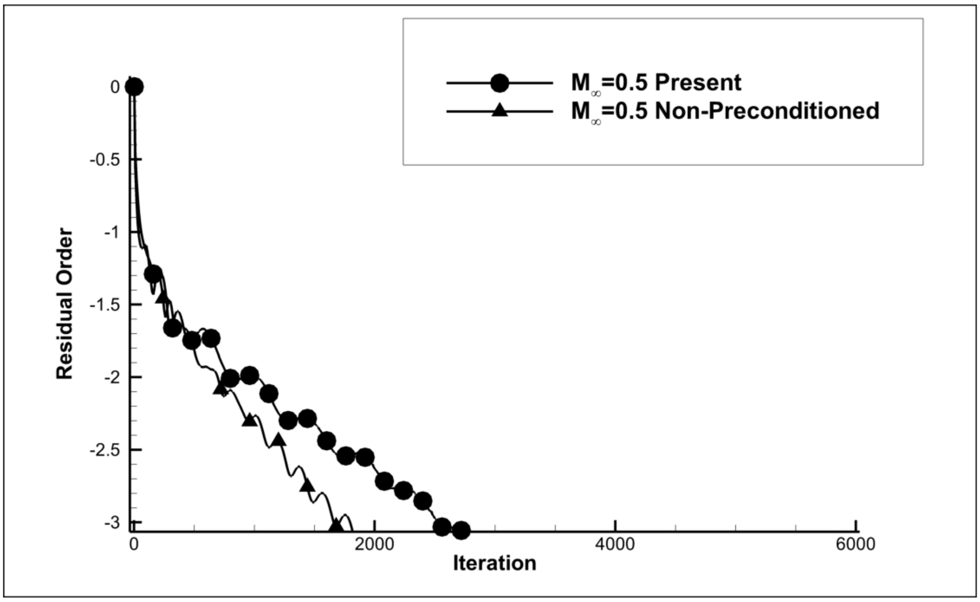

Figure 3.39: Residual histories for flow over ONERA M6 wing at $M_\infty = 0.5$

The transonic case with $M_\infty = 0.8395$ and $\alpha = 3.06$, which is also used as validation case, is next analyzed and compared with the non-preconditioned solution in terms of convergence speed. The convergence rate of the preconditioned solution still does not degrade at transonic flow conditions.

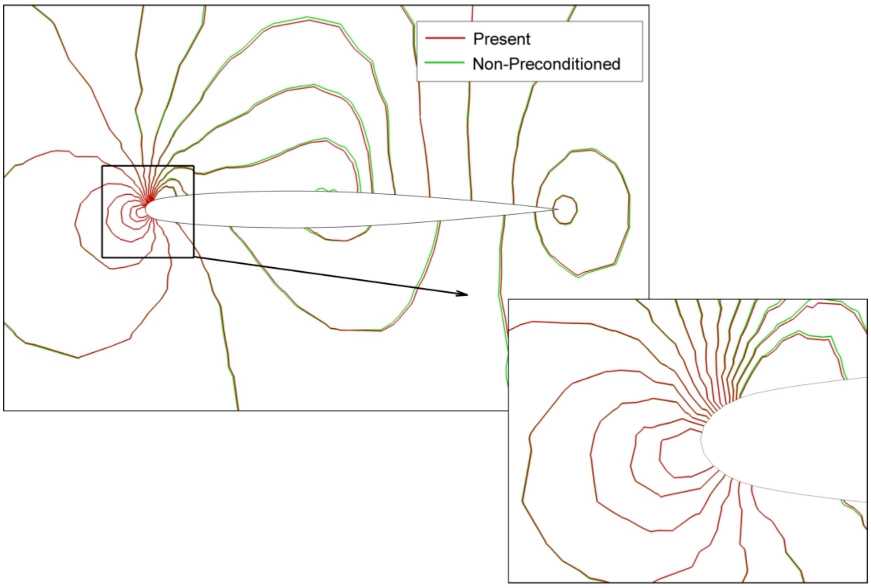

Figure 3.40: Pressure coefficient distributions for flow over ONERA M6 wing at $M_\infty = 0.8395$

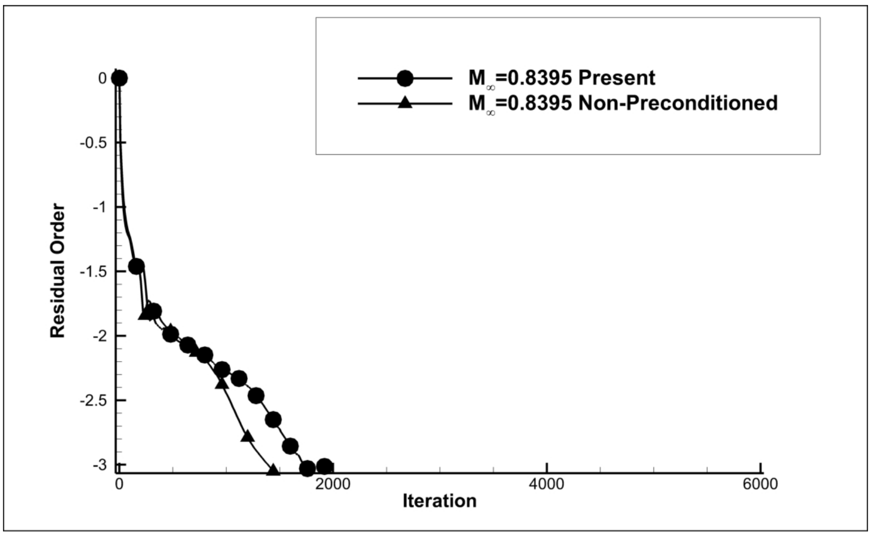

Figure 3.41: Residual histories for flow over ONERA M6 wing at $M_\infty = 0.8395$

It is observed from the results and residual graphs that the present preconditioning matrix has a comparable accuracy and convergence rate with non-preconditioned formulation for all selected flow conditions. Slight differences are attributed to reflecting boundary conditions on the rest of the solutions.

As a special case of $M_\infty = 0.005$ condition, the non-preconditioned solution is obtained by employing a CFL value of 0.01 and considerable wiggles are observed in the flow field as shown in Figure 3.32 in contrast to the preconditioned solution. Convergence rate of the non-preconditioned formulation also get worse when compared with the preconditioned formulation at this case. $M_\infty = 0.005$ is the smallest Mach number for which a non-preconditoned solution can be obtained.

All of the preconditioned solution residuals are also given in Figure 3.42. This figure proves the Mach uniform convergence of preconditioned formulation up to $M_\infty = 0.5$ in inviscid 3-D problems which is consistent with the 2-D results.

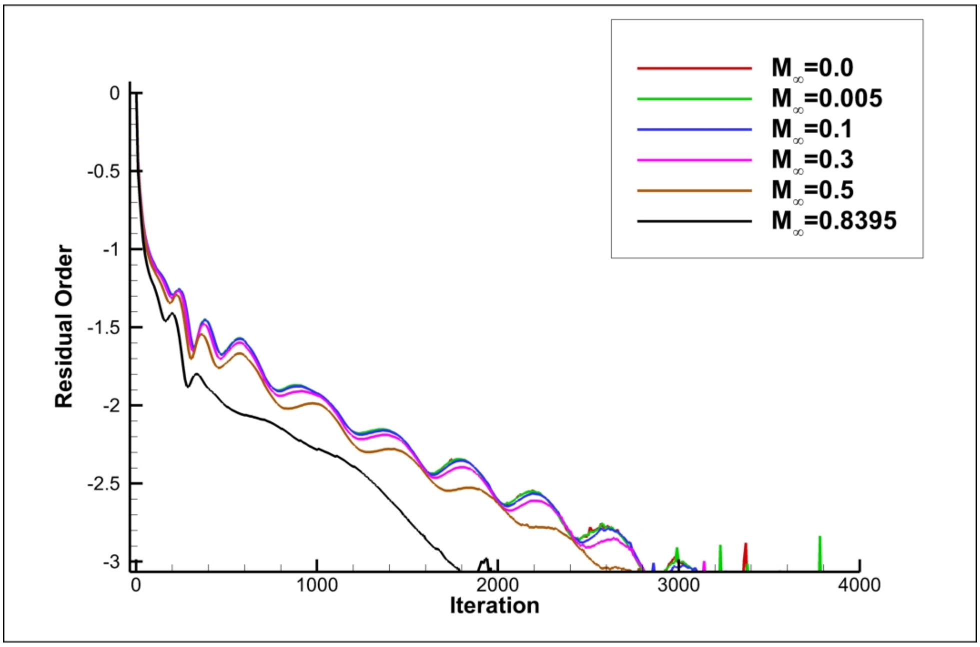

Figure 3.42: Residual histories for flow over ONERA M6 wing

3.2.2 Viscous Flows over DLR-F4 Geometry

Low Reynolds number laminar flows over DLR-F4 geometry are selected as the 3-D viscous test cases. DLR-F4 is a standardized wing-body configuration based on AGARD 303 Report [75] and is widely used in drag prediction workshops since 2001. In this study, the wing-body configuration without the tail is selected as shown in Figure 3.43.

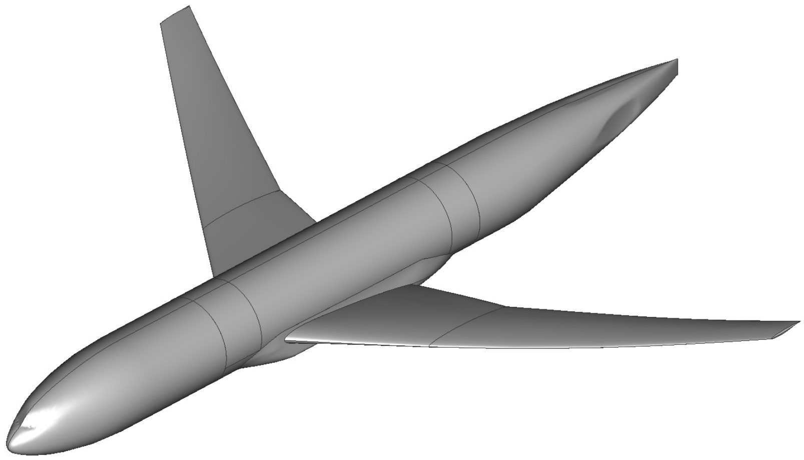

Figure 3.43: DLR-F4 wing-body configuration

A hybrid unstructured grid which consists of 2428821 cells including 1529180 prisms and 899641 tetrahedral is generated with the commercial grid generator GAMBIT^{TM} (Figure 3.44). In the hybrid grid, 20 rows of prismatic elements are used next to the wall boundaries to resolve the boundary layer flow. A slice over the wing-body geometry is given in Figure 3.45 to show the mesh distribution in the direction normal to the solid surfaces.

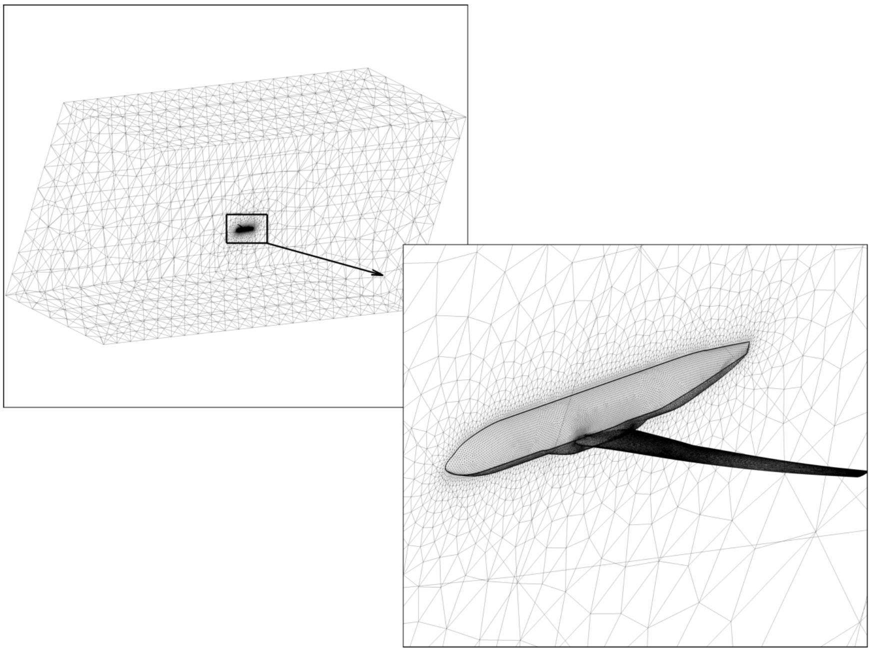

Figure 3.44: Computational grid employed for DLR-F4 wing-body test case

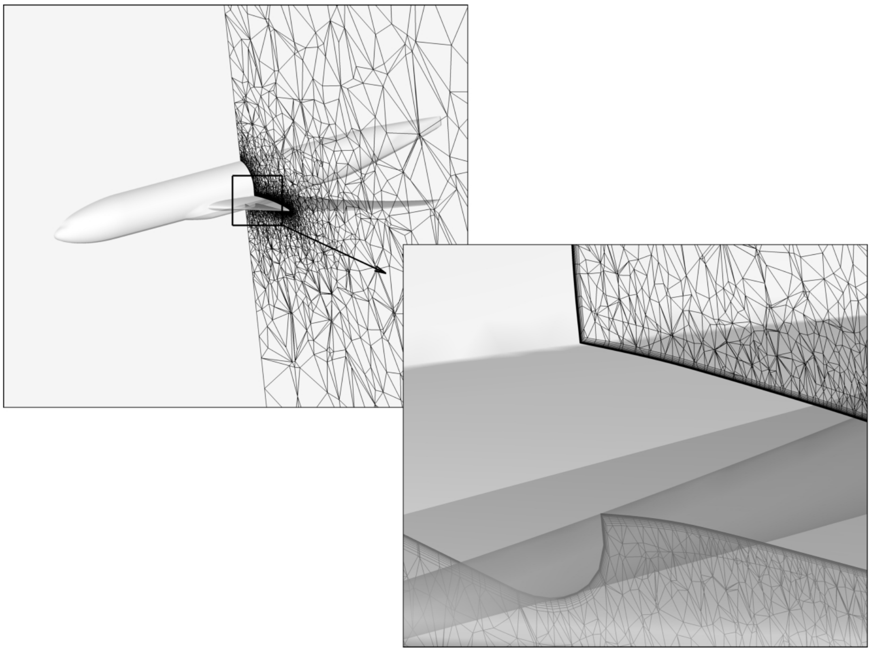

Figure 3.45: Slice of the employed grid for DLR-F4 wing-body test case

In this study, the Reynolds number is kept constant at a value of 250000 with respect to the wing root chord length while the free stream Mach number is changed in the selected test cases. The angle of attack is also fixed at 1°. In all the cases studied, the CFL value is kept at its highest values as long as the numerical solution is stable. The results are compared with the solutions obtained using the commercial flow solver FLUENT® with the same grid and flow conditions. The selected discretization schemes of FLUENT® are similar to HYP3D where the Roe upwinding and the Runge Kutta time stepping are used for spatial and temporal discretizations respectively.

As the first laminar 3-D case, $M_\infty = 0.01$ is solved and the pressure coefficient distributions over the wing-body geometry are compared with the preconditioned solution obtained with FLUENT® and non-preconditioned solution. The pressure coefficient distributions on upper and lower surfaces are shown in Figure 3.46 and Figure 3.47 respectively. The result obtained with present method agrees well with the FLUENT® predictions. On the other hand, the accuracy loss and fluctuations in the flow field is observed in the non-preconditioned solution especially near the wing body junction.

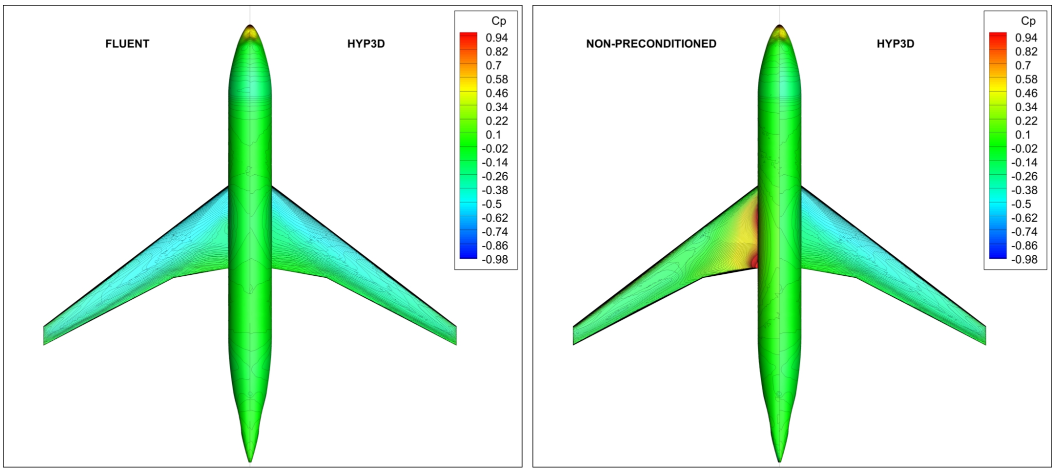

Figure 3.46: Pressure coefficient distribution on DLR-F4 upper surface at $M_\infty = 0.01$

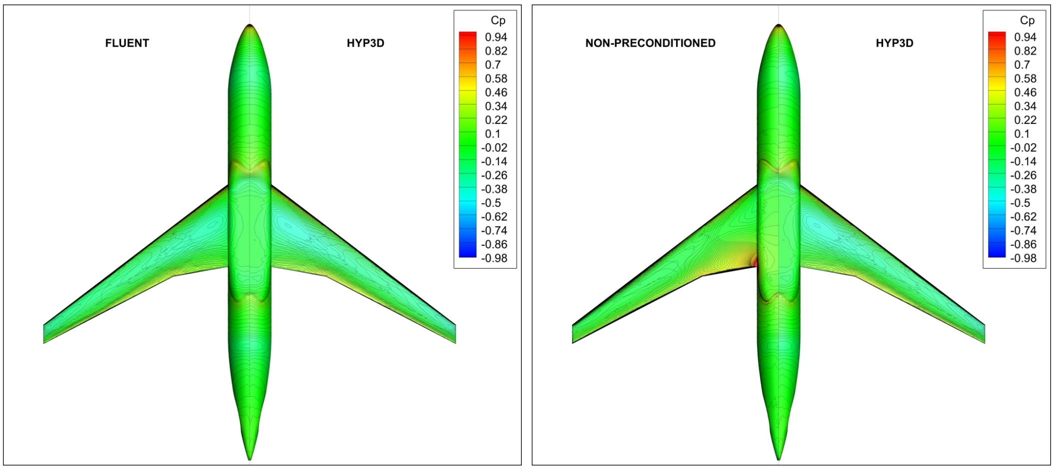

Figure 3.47: Pressure coefficient distribution on DLR-F4 lower surface at $M_\infty = 0.01$

The sectional surface pressure distributions are extracted at 0.2, 0.5 and 0.8 span locations for both solutions and are compared in Figure 3.48, Figure 3.49 and Figure 3.50 for a quantitative assessment. The sectional surface pressure distributions are observed to be in good agreement in all spanwise locations.

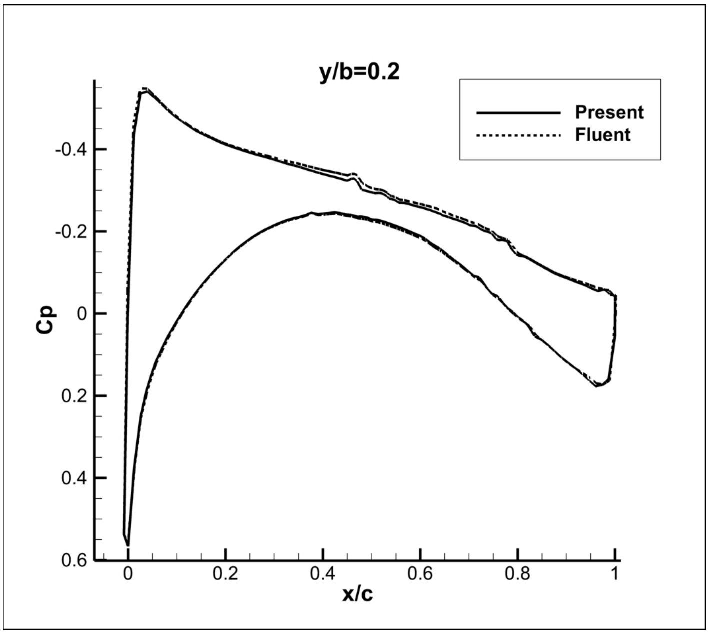

Figure 3.48: Pressure coefficient distribution on 0.2 span at $M_\infty = 0.01$

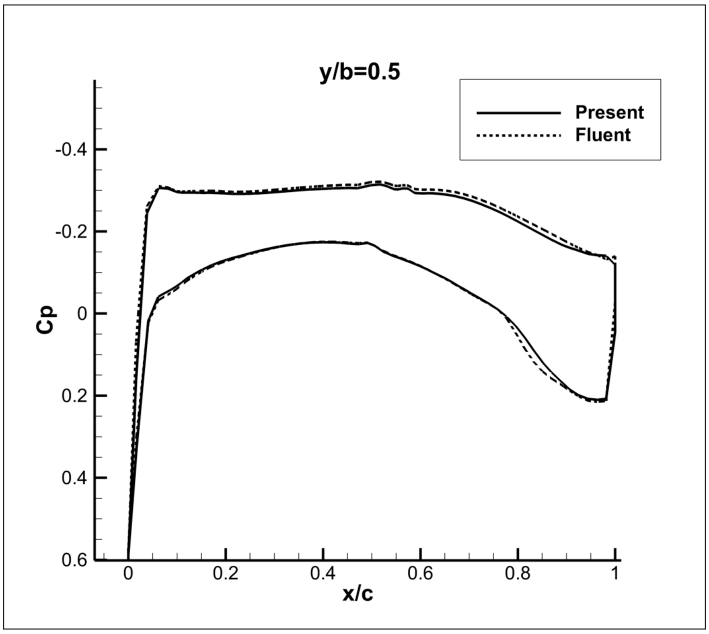

Figure 3.49: Pressure coefficient distribution on 0.5 span at $M_\infty = 0.01$

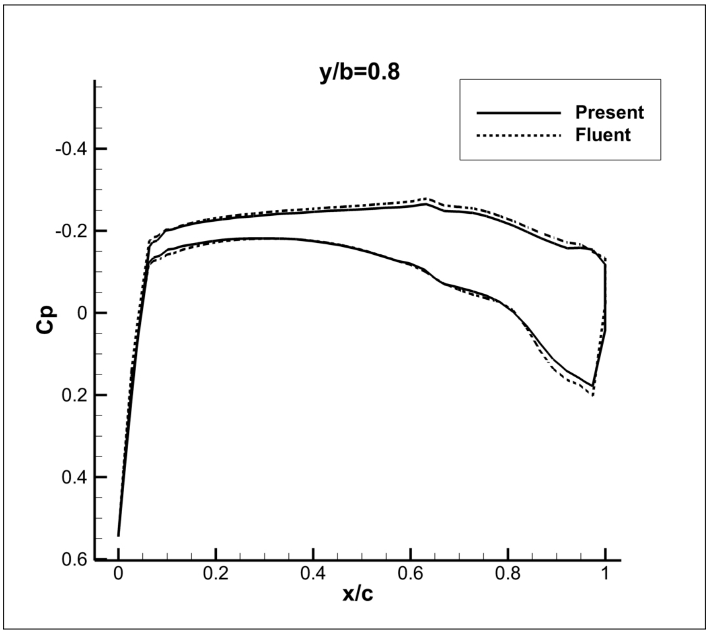

Figure 3.50: Pressure coefficient distribution on 0.8 span at $M_\infty = 0.01$

The residual histories of the solution based on the present method, the non-preconditioned formulation and the FLUENT® are all given in Figure 3.51 for $M_\infty = 0.01$ case. The CFL numbers employed in solutions with the present solver, non-preconditioned solver and FLUENT® are 1.0, 0.1 and 0.17 respectively. They are the highest values with which a stable solution is obtained. The similarities of discretization schemes result in a more reliable comparison and it is observed that the convergence rate of the preconditioned solutions are quite similar. On the other hand, significant fluctuations are observed in the residual history of non-preconditioned solution.

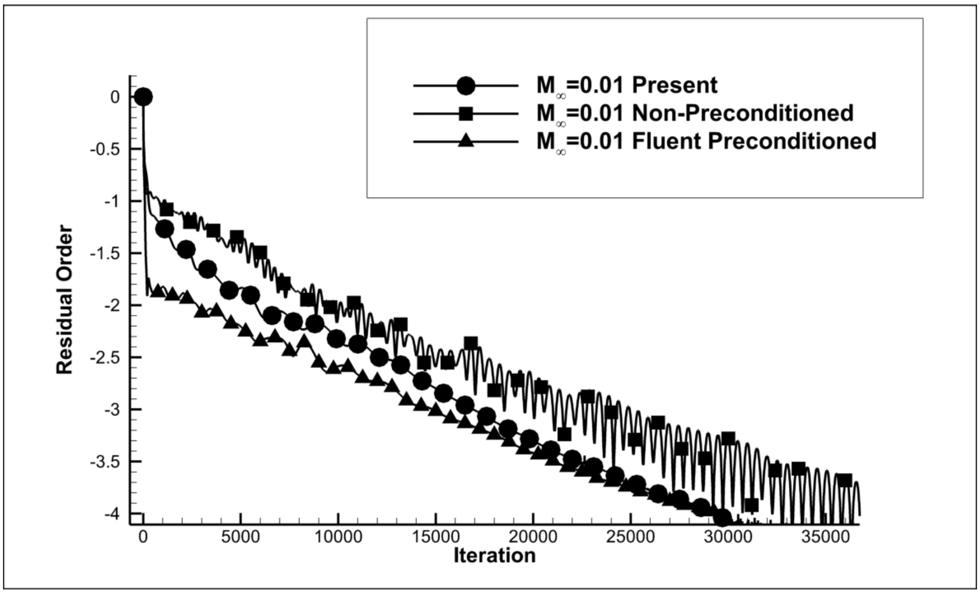

Figure 3.51: Residual histories for flow over DLR-F4 wing-body configuration at $M_\infty = 0.01$

The flow solutions for a range of low Mach numbers including $M_\infty = 0.0$, $M_\infty = 0.1$, $M_\infty = 0.3$ and $M_\infty = 0.5$ are also obtained successfully with the present preconditioning formulation. The residual histories for all the cases are given in Figure 3.52. A Mach uniform convergence rate is similarly observed in the DLR-F4 3-D laminar flow cases.

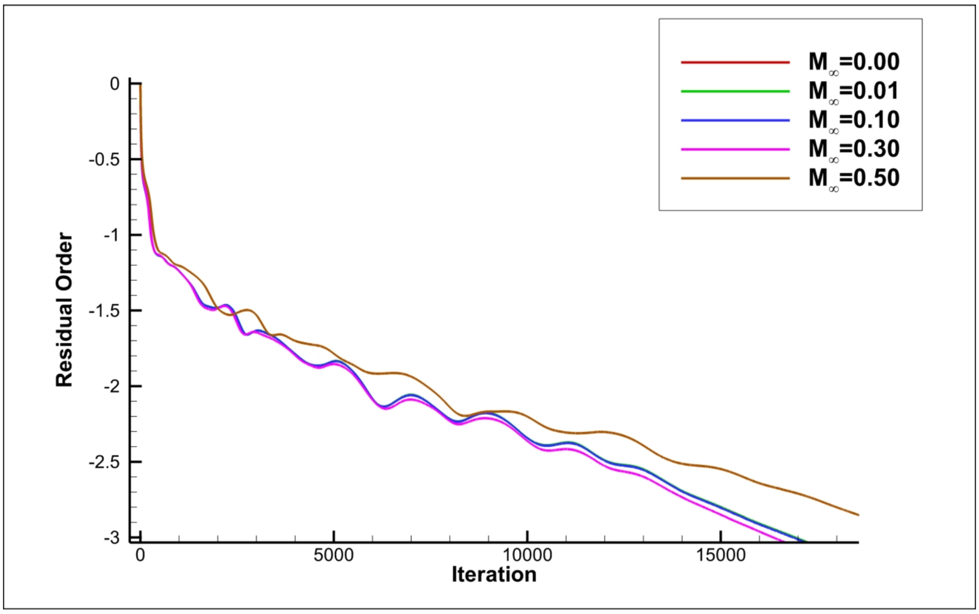

Figure 3.52: Residual histories for flow over DLR-F4 wing-body configuration

CHAPTER 4

CONCLUSION

In this study, a novel preconditioning method for low Mach number flows is developed and validated for 2-D and 3-D inviscid and viscous flows. The preconditioning method is implemented in 2-D and 3-D in-house flow solvers based on finite volume formulation on structured and unstructured grids. The final form of the preconditioning formulation is proved to be grid independent, accurate and stable for low Mach number flows including the zero Mach number case.

First, the Mach uniform preconditioner formulation is validated and its performance is evaluated on 2-D flow cases. For the validation, channel flows with a circular bump and the laminar flow over flat plate with zero pressure gradient are selected. In addition to the validation cases, the performance of the present preconditioning formulation is compared against the non-preconditioned compressible formulation for both inviscid and viscous flows around airfoils. A wide range of Mach number flows including incompressible flows are studied in the performance evaluations both in terms of spatial accuracy and the convergence rate.

Next, the 3-D formulation of the preconditioner is validated for transonic inviscid flows over ONERA M6 wing and a performance evaluation study is conducted at different free stream Mach number flows. Finally, laminar flows over the DLR-F4 wing-body configuration are studied for both validation and performance evaluation of 3-D viscous formulation.

In the 2-D and 3-D cases, the numerical solutions of the preconditioned conservation equations provide the expected stability and convergence acceleration for the solution of subsonic flows including incompressible flows at $M_\infty = 0$. It is shown that the present preconditioner prevents the instability of compressible flow solutions at low Mach numbers and provides a uniform convergence rate for the whole range of subsonic flows. On the other hand, the conservative form of the preconditioned governing equations perform quite similar to the original compressible formulation in transonic flow cases.

When the performance of the present formulation is assessed for viscous flows, no stability or accuracy degradation is observed due to the interaction between preconditioned convective terms and the diffusive terms. Therefore, the present preconditioning formulation requires no modification for the computation of low Mach number viscous flows.

The main contribution of the present study is the proposition of a novel approach to the numerical solution of low speed flows where conservation of energy equation is used to obtain divergence free velocity field. The resulting preconditioned system of equations becomes equivalent to the ACM formulation at the limiting case of $M_\infty = 0$. Yet, the conservative form of the governing equations ensures the stability and the accuracy of transonic flow solutions. The Mach uniform convergence rate achieved in the present formulation is similar to that of the ACM not only for incompressible flows, but also for low subsonic flows.

The present formulation developed can be used with convergence acceleration methods such as multigrid and GMRES to further accelerate the convergence rate of numerical solutions. In addition, the convergence rate of the present preconditioning algorithm is expected to benefit significantly from an implementation of non-reflecting numerical boundary conditions.

REFERENCES

[1] Drikakis D., Rider W., High resolution methods for incompressible and low-speed flows. Springer:Berlin Heidelberg, 2005.

[2] Patel S., Drikakis D., Effects of preconditioning on the accuracy and efficiency of incompressible flows. Int. J. Numerical Methods in Fluids 2005;47:963-970.

[3] Justesen P.,A numerical study of oscillating flow around a circular cylinder. Journal of Fluid Mechanics 1991;222:157-196.

[4] Osswald GA., Ghia KN., and Ghia U., A direct algorithm for solution of incompressible three-dimensional unsteady Navier-Stokes equations. AIAA Paper 1987;87-1139.

[5] Ahn HT., A new incompressible Navier-Stokes method with general hybrid meshes and its application to flow/structure interaction. PhD Thesis, Dept. Of Aerospace Engineering and Engineering Mechanics, The University of Texas, 2005.

[6] Harlow FH., Welch JE., Numerical calculation of time-dependent viscous incompressible flow with free surface. Physics of Fluids 1965;8:2182-2189.

[7] Chorin AJ., Numerical solution of the Navier-Stokes equations. Math. Comp 1968;22:742-762.

[8] Patankar SV., Spalding DB., A Calculation Procedure for Heat, Mass and Momentum Transfer in Three-Dimensional Parabolic Flows. Int. J. of Heat and Mass Transfer 1972;15:1787-1805.

[9] Hafez MM., Numerical simulation of incompressible flows. World Scientific Pub. Co. Inc., 2003.

[10] Temam R., Une methode d'approximation des solutions des equations Navier-Stokes. Bull. Soc. Math. 1968;98:115-152.

[11] Kobayashi M., Pereira C., Calculation of incompressible laminar flows on a nonstaggered, nonorthogonal grids. Num. Heat Transfer 1991;19:243-262.

[12] Peric M., Analysis of pressure-velocity coupling on non-orthogonal grids. Num. Heat Transfer 1990;17:63-82.

[13] Rhie CM., Chow WL., Numerical study of the turbulent flow past an airfoil with trailing edge seperation. AIAA Journal 1983;21:1525-1532.

[14] Patankar SV., Numerical Heat Transfer and Fluid Flow. Hemisphere:New York, 1980.

[15] Vandoormaal JP., Raithby GD., Enhancement of the Simple Method for Predicting Incompressible Fluid Flows. Numerical Heat Transfer 1984;7:147-163.

[16] Spalding DB., Internal Report HTS/80/1. Mechanical Engineering Department, Imperial College of Science Technology and Medicine, London, 1980.

[17] Issa RI., Solution of the implicitly discretized fluid flow equations by operator splitting. J of Comp Phys 1986;62:40-65.

[18] Chorin AJ., A numerical method for solving incompressible viscous flow problems. J of Comp Phys 1967;2:12-26.

[19] Steger JL., Kutler P., Implicit finite-difference procedures for the computation of vortex wakes. AIAA Journal 1977;15:581-590.

[20] Kwak D., Chang JLC., Shanks SP., and Chakravarty S., A three-dimensional incompressible Navier-Stokes flow solver using primitive variables. AIAA Journal 1986;24:390-396.

[21] Chang JLC., Kwak D., Rogers SE., and Yang RJ., Numerical simulation methods of incompressible flows and an application to the space shuttle main engine. Int. J. Numerical Methods in Fluids 1988;8:1241-1268.

[22] Rahman MM., Siikonen T., An artificial compressibility method for viscous incompressibility and low Mach number flows. Int. J. Numerical Methods in Engineering 2008;75:1320-1340.

[23] Liang C., Chan A., Liu X., and Jameson A., An artificial compressibility method for the spectral difference solution of unsteady incompressible Navier-Stokes equations. AIAA Paper 2011;48-449.

[24] Bas O., Development of an incompressible Navier-Stokes solver with alternating cell direction implicit method on structured and unstructured quadrilateral grids. MSc. Thesis, Middle East Technical University 2007.

[25] Karki KC., Patankar SV., Pressure based calculation procedure for viscous flows at all speeds in arbitrary configurations. AIAA Journal 1989;27:1167-1174.

[26] Demirdzic I., Lilek Z., and Peric M., A collocated finite volume method for predicting flows at all speeds. Int. J. for Num. Meth. 1993;16:1029-1050.

[27] McGuirk JJ., Paige GJ., Shock capturing using a pressure correction method. AIAA Journal 1990;28:1751-1757.

[28] Turkel E., Preconditioning methods for solving the incompressible and low speed compressible equations. J of Comp Phys 1987;72:277-298.

[29] Choi Y., Merkle C., The application of preconditioning in viscous flows. J of Comp Phys 1993;105:207-223.

[30] Weiss J., Smith W., Preconditioning applied to variable and constant density flows. AIAA Journal 1995;33:2050-2057.

[31] Van Leer B., Lee WT., and Roe PL., Characteristic time-stepping or local preconditioning of the Euler equations. AIAA Paper 1991;91-1552.

[32] Turkel E., Preconditioning techniques in computational fluid dynamics. Annual Reviews in Fluid Mechanics 1999;31:385-416.

[33] Turkel E., Vatsa VN., Local preconditioners for steady state and dual time-stepping, mathematical modeling and numerical analysis. ESAIM: M2AN 2005;39(3):515-536.

[34] Buelow P., Venkateswaran S., and Merkle CL., The effect of grid aspect ratio on convergence. AIAA 12th Computational Fluid Dynamics Conference 1995.

[35] Venkateswaran S., Merkle CL., Analysis of time derivative preconditioning for the Navier-Stokes equations. 6th Symposium on Computational Fluid Dynamics 1995.

[36] Dohyung L., The design of local Navier-Stokes preconditioning for compressible flow. J of Comp Phys 1998;144:460-483.

[37] Godfrey AG., Topics on spatially accurate methods and preconditioning for the Navier-Stokes equations with finite chemistry. PhD Thesis VPI and SU 1992.

[38] Godfrey AG., Steps towards a robust preconditioning. AIAA Paper 1994;94-0520.

[39] Godfrey AG., Walters RW., and van Leer B., Preconditioning for the Navier-Stokes equations with finite-rate chemistry. AIAA Paper 1993;93-0535.

[40] Colin Y., Deniau H., and Boussuge JF., A robust low speed preconditioning formulation for viscous flow computations. Computers and Fluids 2011;47:1-15.

[41] Merkle CL., Choi YH., Computation of low-speed compressible flows with time-marching procedures. Int. J. Numerical Methods in Fluids 1988;25:293-331.

[42] Lee SH., Cancellation problem of preconditioning method at low Mach numbers. J of Comp Phys 2007;225:1199-1210.

[43] Bas O., Tuncer IH. and Kaynak U., A Mach-uniform preconditioner for incompressible and subsonic flows. Int. J. Numerical Methods in Fluids 2014;74:100-112.

[44] Bas O., Tuncer IH., A 3-D Mach-uniform preconditioner for incompressible and subsonic flows. ECFD VI Paper 2014; 3808.

[45] Stokes GG., On the theories of internal friction of fluids in motion. Transactions of the Cambridge Philosophical Society 1845;9:287-305.

[46] Jameson A., Time dependent calculations using multigrid with application to unsteady flows past airfoils and wings. AIAA Paper 1991;91-1596.

[47] Peyret R., Unsteady evolution of a horizontal jet in a stratified fluids. J of Fluid Mech 1976;78:49-63.

[48] Merkle CL., Athavale M., Time-accurate unsteady incompressible flow algorithms based on artificial compressibility. AIAA Paper 1987;87-1137.

[49] Rogers SE., Kwak D., An upwind differencingscheme for the time-accurate incompressible Navier-Stokes equations. AIAA Paper 1988;88-2583.

[50] Rossow CC., Extension of a compressible code toward the incompressible limit. AIAA Journal 2003;41:12.

[51] Heul DR., Vuik C., and Wesseling P., A conservative pressure-correction method for flow at all speeds. Computers and Fluids 2003;32:1113-1132.

[52] Depcik C., Van Leer B., In search of an optimum local Navier-Stokes preconditioner. AIAA Paper 2003;3703.

[53] Kaya M., Ak MA., and Tuncer IH., An implementation of parallel GMRES solution method on a 3-D unstructured flow solver. 5th AIAC Paper 2009;026.

[54] Ahmet G., Micro-siting of wind turbines using Navier-Stokes solutions coupled with a numerical weather prediction model. PhD. Thesis, Middle East Technical University 2014.

[55] Nigro N., et-all., Physics based GMRES preconditioner for compressible and incompressible Navier-Stokes equations. Computer Meth. in App. Mech. and Eng. 1998;154:203-228.

[56] Vuik C., Solution of the discretized incompressible Navier-Stokes equations with the GMRES method. Int. J. Numerical Methods in Fluids 1993;16:507-523.

[57] Liu C., Zheng X., and Sung CH., Preconditioned multigrid methods for unsteady incompressible flows. J of Comp Phys 1998;139:35-57.

[58] Vierendeels J., Riemslagh K., and Dick E., A multigrid method for viscous incompressible and low speed compressible flows on high aspect ratio grids. Sixteenth Int. Conf. on Num. Meth. in Fluid Dyn. Lecture Notes in Phys. 1998;515:332-337.

[59] Dinçgez U., Three dimensional hyperbolic grid generation. MSc. Thesis, Middle East Technical University 2006.

[60] Richtmyer RD., Morton KW., Difference methods for initial value problems. Wiley-Interscience 2nd Edition London 1967.

[61] Jameson A., Schmidt W., and Turkel E., Numerical solution of the Euler equations by finite volume methods using Runge-Kutta time stepping schemes. AIAA Paper 1981;81-1259.

[62] Maple. Maplesoft, a division of Waterloo Maple Inc., Waterloo, Ontario

[63] Barth TJ., Jespersen DC., The design and application of upwind schemes on unstructured meshes. AIAA Paper 1989;89-0366.

[64] Riemann B., Ueber die fortpflanzung ebener luftwellen von endlicher schwingungsweite. Abhandlungen der Königlichen Gesellschaft der Wissenschaften zu Göttingen 1860.

[65] Li HG., Zong N., Lu XY., and Yang V., A consistent characteristic boundary condition for general fluid mixture and its implementation in a preconditioning scheme. Adv. Appl. Math. Mech. 1912;4:72-92.

[66] Darmofal DL., Eigenmode analysis of boundary conditions for the one-dimensional preconditioned Euler equations. ICASE Technical Report 1998.

[67] Jameson A., Schmidt W., and Turkel E., Numerical solution of the Euler equations by finite volume methods using Runge-Kutta time-stepping schemes. AIAA Paper 1981;81-1259.

[68] Karypis G., and Kumar V., A fast and highly quality multilevel scheme for partitioning irregular graphs. SIAM Journal on Scientific Computing 1999;820:359-392.

[69] Sunderam VS., PVM:A framework for parallel distributed computing. Concurrency:Practice and Experience 1990;2:315-339.

[70] Ni RN., A multiple-grid scheme for solving Euler equations. AIAA Journal 1982;20:1565-1571.

[71] Hejranfar K., Kamali-Moghadam, R., Assesment of three preconditioning schemes for solution of the two dimensional Euler equations at low Mach number flows. Int J Numer Methods in Fluids 2012;89:20-52.

[72] Jones DJ., Test cases for inviscid flowfield methods. AGARD AR-211 1985.

[73] Mueller TJ., Fixed and Flapping Wing Aerodynamics for Micro Air Vehicle Applications. American Institute of Aeronautics and Astronautics, 2001.

[74] Redeker G., Pressure distributions on the ONERA-M6 wing at transonic Mach numbers. AGARD AR-138 1979.

[75] Schmitt V., Charpin F., A selection of experimental test cases for the validation of CFD codes. AGARD AR-303 1994.

APPENDIX A

THREE DIMENSIONAL NON-DIMENSIONALIZED GOVERNING EQUATIONS

The non-dimensionalized 3-D Navier-Stokes equations in integral form are given below.

$$\frac{\partial}{\partial t}\int_V \vec{Q}dV + \oint_A (\vec{F}_c - \vec{F}_v)dA = 0 \tag{A.1}$$

where,

$$\vec{Q} = \begin{pmatrix} \rho \\ \rho u \\ \rho v \\ \rho w \\ \rho e_t \end{pmatrix}$$

$$\vec{F}_c = \begin{pmatrix} n_x(\rho u) + n_y(\rho v) + n_z(\rho w) \\ n_x(\rho u^2 + p) + n_y(\rho uv) + n_z(\rho uw) \\ n_x(\rho vu) + n_y(\rho v^2 + p) + n_z(\rho vw) \\ n_x(\rho wu) + n_y(\rho wv) + n_z(\rho w^2 + p) \\ n_x(u(\rho e_t + p + \frac{1}{(\gamma-1)M_\infty^2})) + n_y(v(\rho e_t + p + \frac{1}{(\gamma-1)M_\infty^2})) \\ +n_z(w(\rho e_t + p + \frac{1}{(\gamma-1)M_\infty^2})) \end{pmatrix}$$

$$\vec{F_v} = \begin{pmatrix} 0 \\ n_x\tau_{xx} + n_y\tau_{xy} + n_z\tau_{xz} \\ n_x\tau_{yx} + n_y\tau_{yy} + n_z\tau_{yz} \\ n_x\tau_{zx} + n_y\tau_{zy} + n_z\tau_{zz} \\ n_x\Theta_x + n_y\Theta_y + n_z\Theta_z \end{pmatrix} \tag{A.2}$$

The non-dimensional viscous stresses, work of viscous stresses and the heat conduction can be formulated as:

$$\begin{aligned}
\tau_{xx} &= \frac{2}{Re}\left(\frac{\partial u}{\partial x} - \frac{1}{3}\nabla\cdot\vec{v}\right) \\
\tau_{yy} &= \frac{2}{Re}\left(\frac{\partial v}{\partial y} - \frac{1}{3}\nabla\cdot\vec{v}\right) \\
\tau_{zz} &= \frac{2}{Re}\left(\frac{\partial w}{\partial z} - \frac{1}{3}\nabla\cdot\vec{v}\right) \\
\tau_{xy} = \tau_{yx} &= \frac{1}{Re}\left(\frac{\partial u}{\partial y} + \frac{\partial v}{\partial x}\right) \\
\tau_{xz} = \tau_{zx} &= \frac{1}{Re}\left(\frac{\partial u}{\partial z} + \frac{\partial w}{\partial x}\right) \\
\tau_{yz} = \tau_{zy} &= \frac{1}{Re}\left(\frac{\partial v}{\partial z} + \frac{\partial w}{\partial y}\right) \\
\Theta_x &= u\tau_{xx} + v\tau_{xy} + w\tau_{xz} + k\frac{\partial(T)}{\partial x} \\
\Theta_y &= u\tau_{yx} + v\tau_{yy} + w\tau_{yz} + k\frac{\partial(T)}{\partial y} \\
\Theta_z &= u\tau_{zx} + v\tau_{zy} + w\tau_{zz} + k\frac{\partial(T)}{\partial z}
\end{aligned}$$

where,

$$k = \frac{\gamma}{RePr} \tag{A.3}$$

APPENDIX B

THREE DIMENSIONAL PRECONDITIONED FORMULATION

The 3-D version of the present preconditioning method is given below with the eigenvalues and eigenvectors of the resulting system of equations.

$$\frac{\partial \vec{Q}}{\partial t} + \Gamma \left(\frac{\partial (\vec{E}_c - \vec{E}_v)}{\partial x} + \frac{\partial (\vec{F}_c - \vec{F}_v)}{\partial y} + \frac{\partial (\vec{G}_c - \vec{G}_v)}{\partial z} \right) = 0$$

where

$$\vec{Q} = \begin{pmatrix} \rho \\ \rho u \\ \rho v \\ \rho w \\ \rho e \end{pmatrix}$$

$$\vec{E}_c = \begin{pmatrix} \rho u \\ \rho u^2 + p \\ \rho u v \\ \rho u w \\ u \left(\rho e + p + \frac{1}{(\gamma-1) M_\infty^2} \right) \end{pmatrix} , \ \vec{F}_c = \begin{pmatrix} \rho v \\ \rho v u \\ \rho v^2 + p \\ \rho v w \\ v \left(\rho e + p + \frac{1}{(\gamma-1) M_\infty^2} \right) \end{pmatrix}$$

$$\vec{G}_c = \begin{pmatrix} \rho w \\ \rho w u \\ \rho w v \\ \rho w^2 + p \\ w\left(\rho e + p + \frac{1}{(\gamma-1)M_\infty^2}\right) \end{pmatrix}$$

$$\vec{E}_v = \begin{pmatrix} 0 \\ \tau_{xx} \\ \tau_{yx} \\ \tau_{zx} \\ \Theta_x \end{pmatrix} \, , \; \vec{F}_v = \begin{pmatrix} 0 \\ \tau_{xy} \\ \tau_{yy} \\ \tau_{zy} \\ \Theta_y \end{pmatrix} \, , \; \vec{G}_v = \begin{pmatrix} 0 \\ \tau_{xz} \\ \tau_{yz} \\ \tau_{zz} \\ \Theta_z \end{pmatrix}$$

and Γ is the Mach uniform preconditioning matrix:

$$\Gamma = \begin{bmatrix} M_\infty^2 & 0 & 0 & 0 & 0 \\ 0 & 1 & 0 & 0 & 0 \\ 0 & 0 & 1 & 0 & 0 \\ 0 & 0 & 0 & 1 & 0 \\ 0 & (1-M_\infty^2)u & (1-M_\infty^2)v & (1-M_\infty^2)w & M_\infty^2 \end{bmatrix}$$

The eigenvalues, eigenvectors and its inverse for the present 3-D formulation is also given below.

$$\lambda = \begin{pmatrix} u' \\ u' \\ u' M_\infty^2 \\ u' - c \\ u' + c \end{pmatrix}$$

$$R = \begin{pmatrix} 0 & 0 & 1 & M_\infty^2 & M_\infty^2 \\ 0 & 0 & u' & u'-c & u'+c \\ w' & w' & 0 & \frac{v'F}{c} & -\frac{v'G}{c} \\ v' & -v' & 0 & \frac{w'F}{c} & -\frac{w'G}{c} \\ 2w'v' & 0 & \frac{(u'^2-v'^2-w^2)}{2}+\frac{(M_\infty^2-1)u'^2}{(\gamma-1)} & D-E & D+E \end{pmatrix}$$

$$R_1^{-1} = \begin{pmatrix} -\frac{v'^2+w'^2(\gamma-1)q_t}{4v'w'c^2} \\ -\frac{v'^2-w'^2(\gamma-1)q_t}{4v'w'c^2} \\ \frac{J}{2FG} \\ \frac{(\gamma-1)q+2u'c}{4Fc} \\ -\frac{(\gamma-1)q-2u'c}{4Gc} \end{pmatrix}, \quad R_2^{-1} = \begin{pmatrix} \frac{u'v'^2+w'^2H}{2v'w'c^2} \\ \frac{u'v'^2-w'^2H}{2v'w'c^2} \\ -\frac{M^2(\gamma-1)u'}{FG} \\ -\frac{u'H+c}{2Fc} \\ \frac{u'H-c}{2Gc} \end{pmatrix}, \quad R_3^{-1} = \begin{pmatrix} \frac{(\gamma-1)v'^2+w'^2+c^2}{2w'c^2} \\ \frac{(\gamma-1)v'^2-w'^2+c^2}{2w'c^2} \\ -\frac{M^2(\gamma-1)v'}{FG} \\ -\frac{(\gamma-1)v'}{2Fc} \\ \frac{(\gamma-1)v'}{2Gc} \end{pmatrix}$$

$$R_4^{-1} = \begin{pmatrix} \frac{(\gamma-1)v'^2+w'^2+c^2}{2v'c^2} \\ \frac{(\gamma-1)v'^2-w'^2-c^2}{2v'c^2} \\ -\frac{M^2(\gamma-1)w'}{FG} \\ -\frac{(\gamma-1)w'}{2Fc} \\ \frac{(\gamma-1)w'}{2Gc} \end{pmatrix}, \quad R_5^{-1} = \begin{pmatrix} -\frac{(\gamma-1)v'^2+w'^2}{2v'w'c^2} \\ -\frac{(\gamma-1)v'^2-w'^2}{2v'w'c^2} \\ \frac{M^2(\gamma-1)}{FG} \\ \frac{(\gamma-1)}{2Fc} \\ -\frac{(\gamma-1)}{2Gc} \end{pmatrix}$$

where:

$$c = \sqrt{\tfrac{\gamma p M_\infty^2 + 1}{\rho} + (1 - M_\infty^2)u'^2}$$

$$q = u'^2 + v'^2 + w'^2$$

$$A = \gamma^2 + (M_\infty^2 - 4)\gamma + 3 - M_\infty^2$$

$$B = c^2 + (M_\infty^2 - 1)u'^2$$

$$H = (\gamma - 2 + M_\infty^2)$$

$$D = \tfrac{(M_\infty^2 - 1)u'^2 + c^2}{(\gamma - 1)} - \tfrac{(M_\infty^2 - 2)q_t}{2}$$

$$E = u'c - \tfrac{(M_\infty^2 - 1)u'v'^2}{c} - \tfrac{(M_\infty^2 - 1)u'w^2}{c}$$

$$F = (M_\infty^2 - 1)u' + c$$

$$G = (M_\infty^2 - 1)u' - c$$

$$H = (M_\infty^2 + \gamma - 2)$$

$$J = M_\infty^2(\gamma - 1)q_t - u'^2(M_\infty^2 - 1) - 2c^2$$

CURRICULUM VITAE

PERSONAL INFORMATION

Surname, Name: BAŞ, Onur
Nationality: Turkish (TC)
Date and Place of Birth: 19 September 1982, Adana
Marital Status: Married
Phone: +90 (505) 2374628
E-mail: obas@ae.metu.edu.tr

EDUCATION

Degree	Institution	Year of Graduation
M.S.	METU Department of Aerospace Engineering	2007
B.S.	METU Department of Aerospace Engineering	2004
High School	İçel Anadolu Lisesi	2000

PROFESSIONAL EXPERIENCE

Year	Place	Enrollment
2013-Present	TUSAŞ Aerospace Industries	Design Specialist
2010-2013	Roketsan A.Ş.	Specialist Design Engineer
2006-2009	Roketsan A.Ş.	Design Engineer
2005-2006	Turbotek Ltd.Şti.	Design Engineer
2004-2005	TUSAŞ Aerospace Industries	Project Engineer

PUBLICATIONS

International Journal Publications

- Baş O., Tuncer İH. and Kaynak Ü., A Mach uniform preconditioner for incompressible and subsonic flows. Int. J. Numer. Meth. Fluids 2014;74:100-112

International Conference Publications

- Baş O. and Tuncer İH., A 3-D Mach uniform preconditioner for incompressible and subsonic flows. 6th European Conference on Computational Fluid Dynamics (ECFD VI) 2014;2014-3808.
- Baş O., Çakmakçıoğlu SC. and Kaynak Ü., A novel intermittency distribution based transition model for low-Re number airfoils. 31st AIAA Applied Aerodynamics Conference 2013;6:2013-2531
- Baş O., Çete AR., and Tuncer İH., Solution of incompressible Navier-Stokes equations with alternating cell direction implicit method on unstructured quadrilateral grids. AIAC 2007;2007-086